Journal for Occultation Astronomy

Volume 14 · No. 4 2024-04

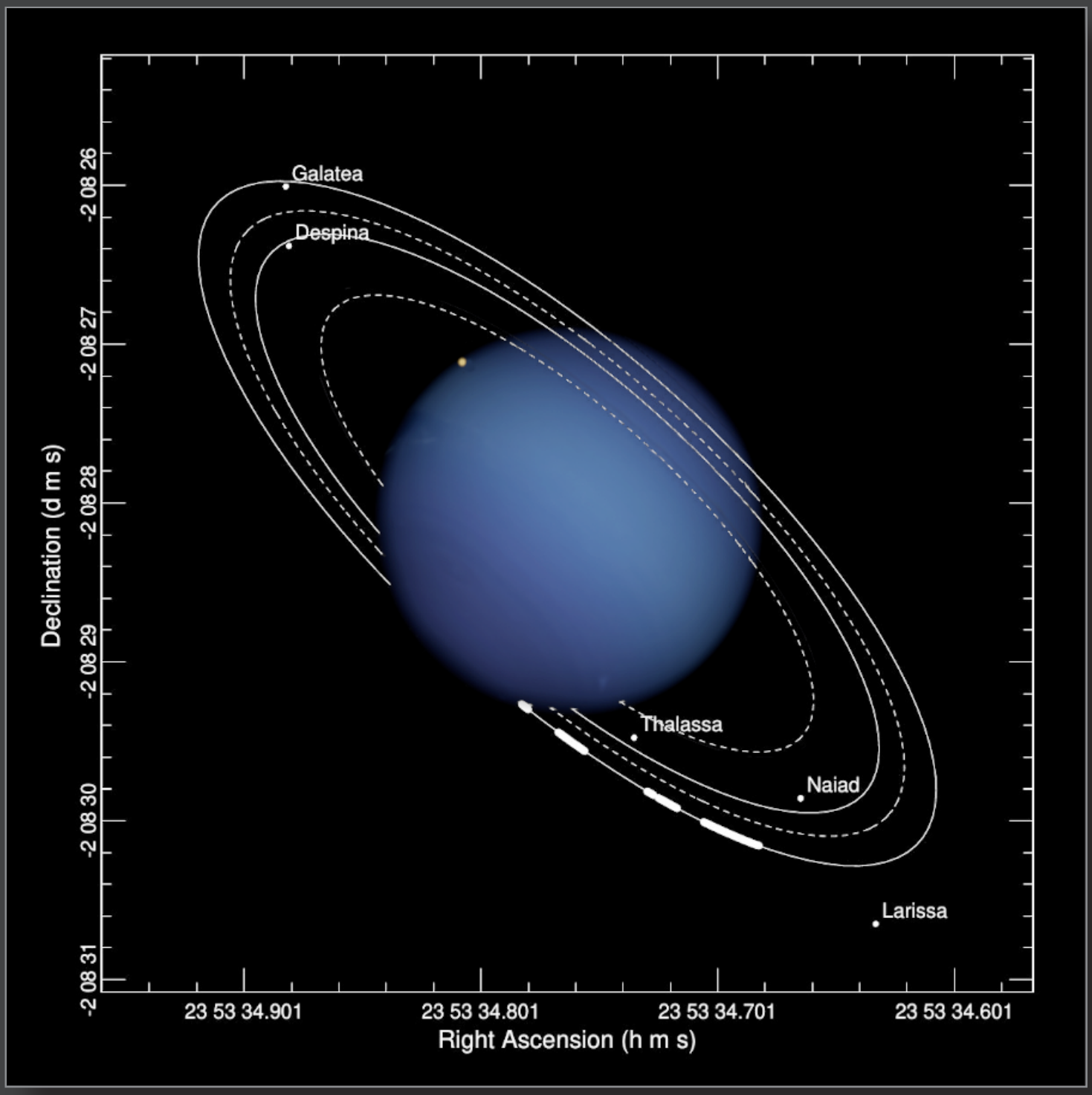

Occultation of UCAC4 440-126076 by Neptune, 2024 Oct 09

Dear reader,

The high accuracy of the predictions of stellar occultations and thus the constantly increasing number of observations represent a major challenge for the observing community worldwide in terms of evaluation and data storage. Since the launch of SODIS (Stellar Occultation Data Input System) in Europe, more than 5,100 observations have been added to the database after processing by the reviewers.

The smooth process requires a lot of time from the reviewer, even in the various reporting systems in America, Asia or Oceania. The careful preparatory work of the observers significantly supports the evaluation by the reviewers. Your observation report should be filled out conscientiously and the light curves prepared with a great deal of patience. Don't forget: You too have taken your first steps in this interesting field of astronomy in the past and have certainly sought advice from others. Experienced observers should help 'rookies' with the preparation and reporting of observations. Please become active here.

In addition, you can help the community in developing software and hardware, in analysing observations and writing reports and articles to the *Journal for Occultation Astronomy*. This issue gives you some fine examples.

And most importantly: Tell others about your enthusiasm for observing occultations - we are counting on you!

Oliver Klös

IOTA/ES, Public Relations

COVER

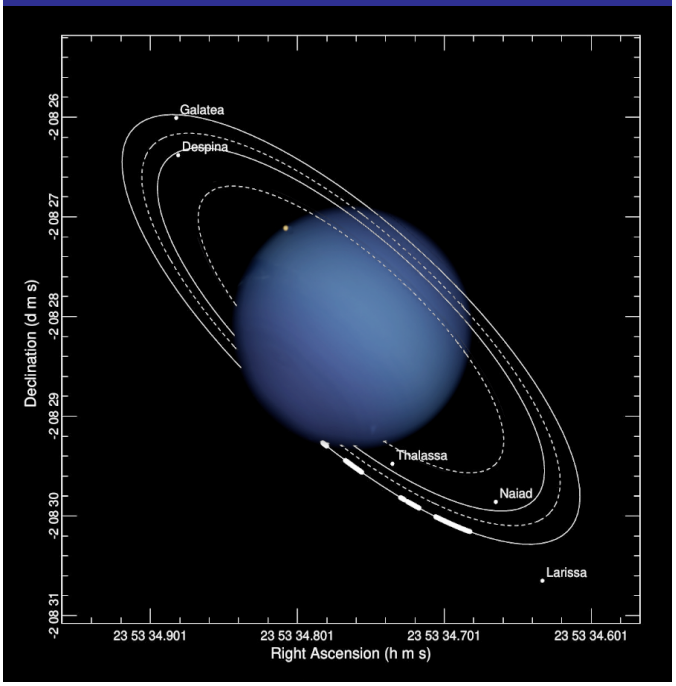

The graphic on the cover shows the egress of UCAC4 440-12607 (11.4 mag) on Neptune on 2024 October 9, 00:48 UT, from the geographical location of N50°, E 10°. The graphic was generated with *Neptune Viewer Tool 3.1* from NASA's Planetary Data System and was enhanced with a simulated image of Neptune from *Stellarium 23.3*. Notes to a successful observation of this event can be found on W. Beisker's Call for Observations. (Graphic: O. Klös)

JOA Volume 14 · No. 4 · 2024-4 $ 5.00 · $ 6.25 OTHER (ISSN 0737-6766)

In this Issue:

Copyright Transfer

Rules for Authors

In order to optimise the publishing process, certain rules for authors have been set up how to write an article for *JOA*. They can be found in "How to Write an Article for *JOA*" published in this *JOA* issue (2018-3) on page 13. They also can be found on our webpage at https://www.iota-es.de/how2write_joa.html .

Journal for Occultation Astronomy

Experimentally Assessing the Accuracy of Eclipse Path Maps

Luca Quaglia · Sydney, New South Wales · Australia · besselianelements@gmail.com
John Irwin · Guildford, England · United Kingdom · john@jir1667.plus.com
Alessandro Pessi · Milan · Italy · issepela@gmail.com

ABSTRACT: Several online eclipse maps were made available in the run-up to the 2024 April 8th total solar eclipse. However, close inspection of these maps quickly revealed notable and significant discrepancies in the location of umbral shadow path limits. These differences can sometimes amount to a couple of kilometres or more. To address the question of eclipse map accuracy, we analyse some relevant observational data collected during this eclipse and provide insights on the factors that affect such accuracy.

Introduction

The umbral path of the 2024 April 8th total solar eclipse (TSE2024) crossed Mexico, the continental US and Canada. Millions of people heavily relied on online eclipse maps to plan their expeditions to the path of totality. While most observers headed for the eclipse centreline or locations well within the path, some found themselves, for all sorts of reasons, near the umbral shadow path limits. Some were trying to flee overcast skies, some had family or friends living near the eclipse path edges, many simply dwelled, studied or worked in those locations. All these observers, and all those communities bisected by the totality path limits, had to rely on the accuracy of predicted eclipse limits to assess if they were going to be in the path of totality.

Below we will take a detailed look at one observation undertaken from a site located close to the path limit and use it to assess how well the predictions stand up. We will also examine two other observations from the eclipse edge in light of the results gathered from the main observation. This analysis includes a comprehensive array of predictions and observations made by the authors, which we will use as a baseline for the comparisons.

Comparing Eclipse Predictions

The Besselian Elements Team (of which the authors are a part) observed the eclipse from Stephenville, TX (USA). Figure 1 provides a comparison of the northern limit lines predicted by several online sources for this location, highlighted with the following colours:

- timeanddate.com [1]
- (full) xjubier.free.fr [2]
- eclipse2024.org [3]
- svs.gsfc.nasa.gov [4] (specifically upath_high.kml)
- (dashed) xjubier.free.fr (inferred by building the locus of points having zero seconds of limb-corrected duration)
- besselianelements.com [5]

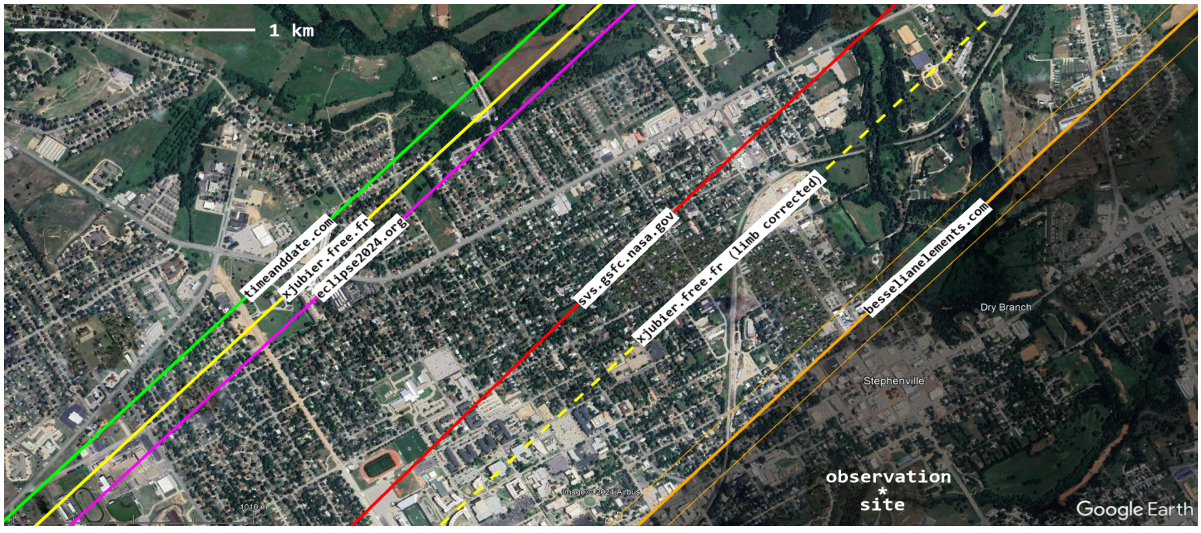

Figure 1. Comparison of various online predictions of the eclipse northern limit at Stephenville, TX. Also displayed is the location of the Besselian Elements Team observation site.

The last prediction was computed by John Irwin based on a robust eclipse computational model which accounted for the topography of the Earth and Moon and used an improved value for the eclipse solar radius (959.95" at one au). The two thin lines surrounding the orange one depict the variation in the location of the northern limit due to the measured uncertainty (±0.05") in the eclipse solar radius. These results are based on the work reported in [6].

We will recall that, because the Sun is not a solid body, the edge of the photosphere is not sharply defined. Thus there is no unambiguous definition of the solar radius and the eclipse limits are affected by some degree of fuzziness. Hence we prefer to use the idea of the *eclipse solar radius*, by which we only mean the parameter that we need to use in precise eclipse computations to reproduce as closely as possible the observations (such as the duration of totality). It is worth remembering that computations are always performed in this way, by assuming that the Sun is a perfect sphere with a sharp edge. Consequently, this parameter will always be affected by some uncertainty due to the fuzzy nature of the Sun's edge. Further considerations on this subject can be found in [6].

Direct measurement of the location of the eclipse limits would then be an arduous task. Discriminating between extremely short totality and no totality at all is very challenging and becomes more and more difficult the closer one gets to the limit. Moreover, it would require many recording devices to be positioned orthogonally with respect to the limit. We can nevertheless indirectly gauge the location of the limit by measuring the duration of totality by timing, as accurately as possible, 2nd and 3rd contacts (a relatively easier task than directly locating the position of the limit).

Contact timing is also affected by the implications of the fuzzy-edged Sun and, of course, by experimental errors. Uncertainties can amount to 1-2 s, but by observing very close to the edge of totality their impact is greatly lessened. Under these circumstances, as shown in Figure 2a, the totality duration varies rather rapidly by moving away from the eclipse limit – in this case by ~21 s/km immediately inside the limit line. Figure 2a was computed specifically for the neighbourhood of the observing site in Stephenville by relying on the above-mentioned robust eclipse computational model. Changes in slope are not an artifact but are caused by the fact that the lunar valleys determining 2nd and 3rd contacts change as one moves away from the eclipse limit.

Figure 2a should be compared with Figure 2b which depicts the variation of the totality duration in the neighbourhood of the centreline (both figures are computed for the same maximum eclipse time). The variation is now far more muted (<1 s/km). For the same level of uncertainty, a measurement of totality duration performed very near the limits is far more sensitive to the distance of the observer from the limit, or conversely, to the distance of the limit from the observer.

Methods

We timed the contact times manually by visually observing the eclipse flash spectrum through 1000 lines/mm diffraction grating spectacles by Rainbow Symphony and using a purpose-built UTC Event Timer device (shown in Figure 3). This device is based on an Arduino UNO board, a GPS and SD Card shield, and a GPS receiver antenna. Once powered up the device records the UTC time when a button is pressed and saves it to the SD card. The events that we were looking for were first, the disappearance, and then the reappearance, of the photospheric continuum in the flash spectrum. We successfully conducted a similar experiment during ATSE2023 [7].

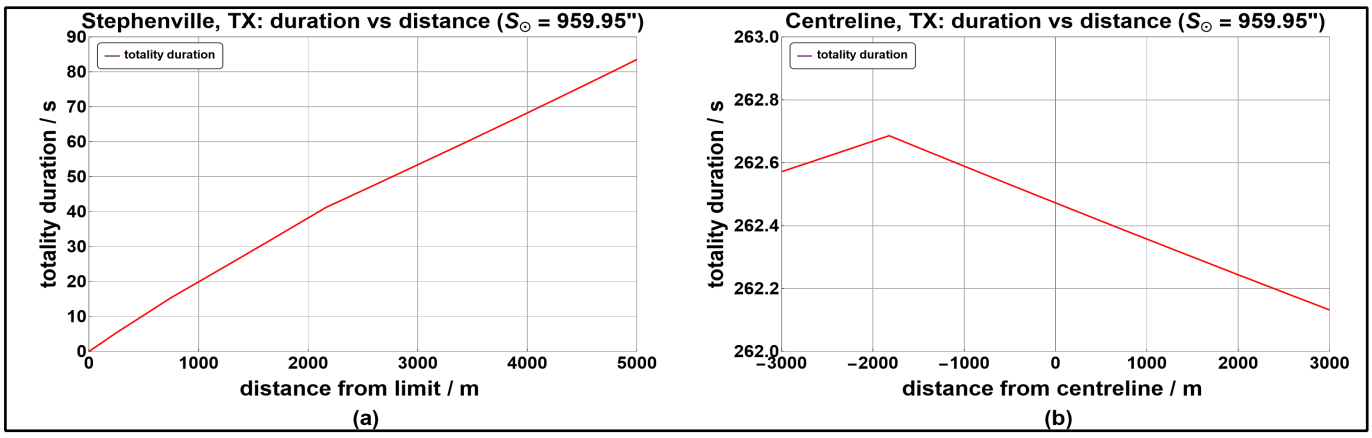

Figure 2a,b. On the left, duration of totality as a function of the distance inside the northern path limit at Stephenville. On the right, as a function of the distance from the centreline for locations experiencing maximum eclipse at the same time as Stephenville. Durations take into account the true topocentric lunar limb as seen from the respective sites. Changes in slope are due to 2nd or 3rd contact occurring at a different lunar limb valley as the distance from the limit or the centreline changes. Note the wildly different scales used on the y-axes and how the longest duration is offset from the centreline. Data sampling interval = 100 m.

Figure 3. UTC Event Timer.

We also recorded the flash spectrum with a QHY174-M CCD camera and a Canon EF 24-105mm f/4L IS USM lens, connected via a Cyclops Optics Blade-C camera lens adapter. Its ability to accurately timestamp the start and the end of each image exposure is a very attractive feature of this camera. The exposure was set at 20 ms and the gain to ~400. We managed to record FITS files at ~12.5 Hz, which is an adequate frame rate, faster than the timescale of eclipse evolution, especially near the path limits where phenomena occur at a much slower rate than closer to the centreline.

Figure 4 shows a section of the flash spectrum recorded around maximum eclipse when the eclipse was unequivocally total, and the photosphere had vanished. We can see in the image the bright emission arcs of hydrogen at 486.1 nm (Balmer's Hβ line) and helium at 587.6 nm. Other emission lines are highlighted, such as the magnesium triplet (at 516.7 nm, 517.3 nm and 518.4 nm) and the sodium doublet (at 589.0 nm and 589.6 nm) just next to the helium line. Indicated with arrows, we can see the ghostly glow of the 530.3 nm Fe XIV emission from the inner corona. Also visible are faintly luminous thin bands running longitudinally along the flash spectrum and marked by the letters A, B, C, and D. These are due to a forest of very faint emission lines coming from the mesosphere, the lowermost layer of the solar atmosphere, only about 500 km thick, and just above the photosphere.

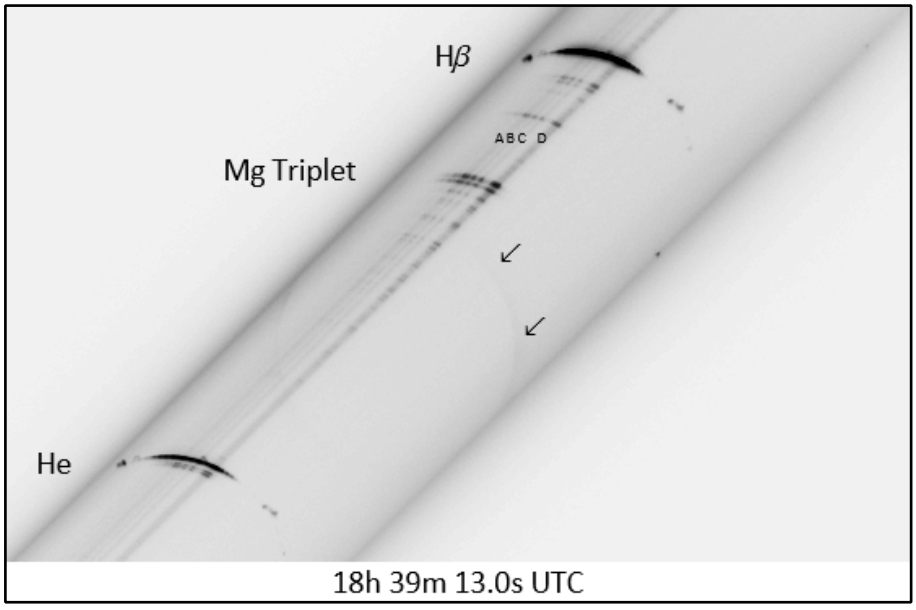

Figure 4. Image of the eclipse flash spectrum recorded with the QHY 174-M CMOS camera around the time of maximum eclipse at Stephenville. Indicated are some of the more conspicuous emission lines. The arrows highlight the very faint ghostly spectrum of the inner corona. Refer to Figure 5 for the meaning of the letters A, B, C, and D. The grayscale image has been reversed and sharpened to better highlight structure in the flash spectrum.

The position of these thin bands corresponds to valleys on the lunar limb. Figure 5 shows the predicted relative motion of the solar and lunar limbs as seen from Stephenville and identifies these lunar valleys. The simulation (like all subsequent ones) is based on our accurate eclipse computational model. A consequence of these dynamics is that, for several seconds after 2nd contact, faint mesospheric light was shining through the lunar valleys marked with the letters A, B and C. Meanwhile, mesospheric light was already starting to appear just above the complex of lunar valleys marked by D. Due to the way the solar limb was moving towards this lunar valley complex, we expected the mesospheric band marked with D to be a little thicker and brighter than the other ones. This is confirmed in the flash spectrum image shown in Figure 4.

Observations and Discussion

We observed the eclipse from Stephenville City Park at a site with WGS84 coordinates:

λ = 98° 12′ 09.7" W
φ = 32° 12′ 58.2" N
h = 348 m

The sky conditions at this location were ideal – clear blue sky and no wind. Considering that the meteorological situation in Texas and elsewhere on eclipse day was particularly unfavourable, we were extremely lucky. Thus, the manual timing measurements could be conducted without any interference. The flash spectrum was very sharp viewed through the diffraction grating spectacles and as usual it was breathtaking to see it emerging and evolving.

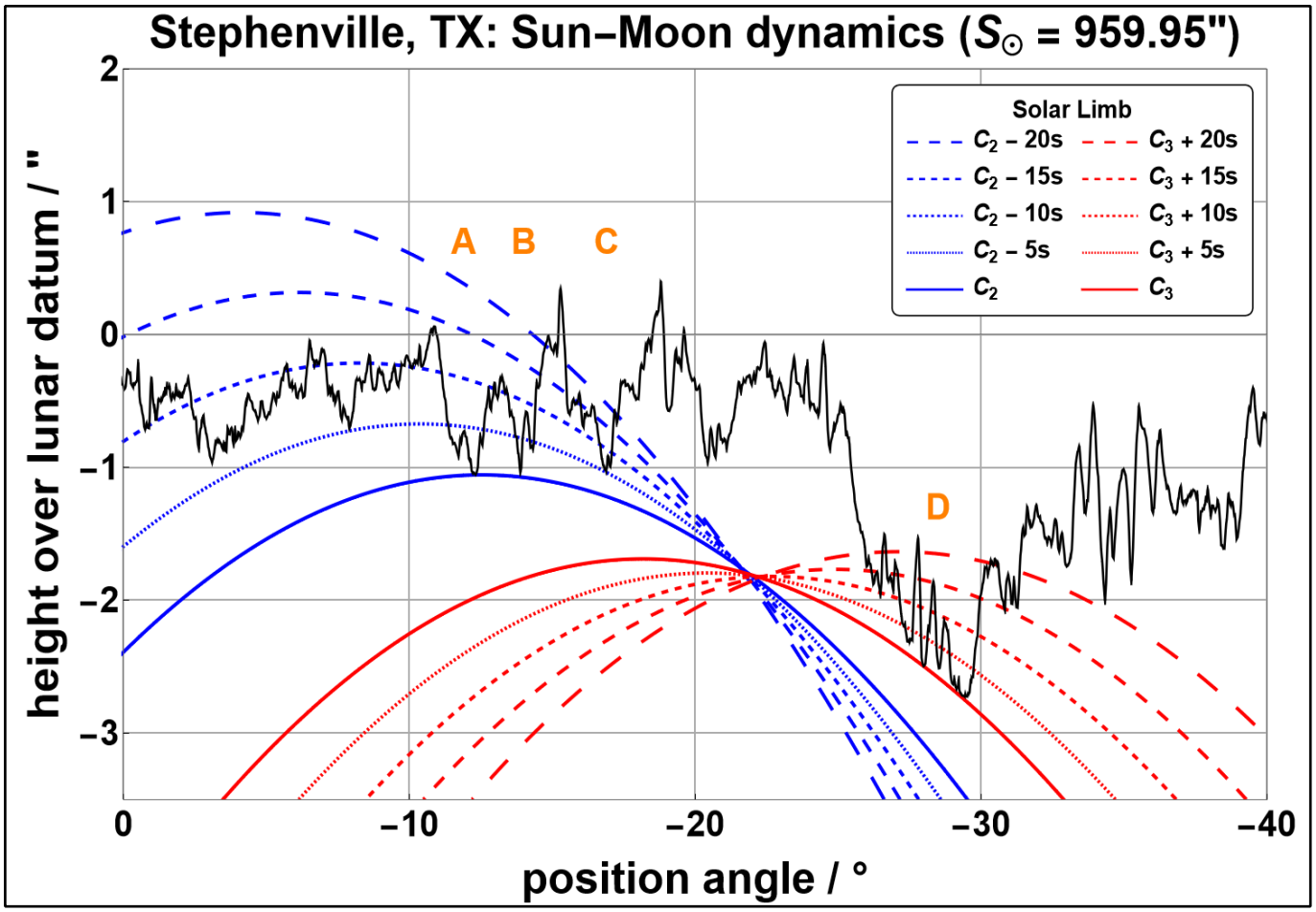

Figure 5. Relative motion of the solar limb with respect to the lunar limb (in black) for the observation site at Stephenville. The lunar limb is drawn as though it were stationary while the solar limb is represented by red and blue lines at different times during the progression of the eclipse. The motion of the Sun with respect to the Moon is from left to right. The inset indicates the position of the solar limb with respect to the times of 2nd and 3rd contact. The lunar valleys marked with the letters A, B, C, and D generate corresponding mesospheric features in the flash spectrum presented in Figure 4. For a time T_0 = 18:39:13 UTC, near mid-eclipse, the apparent topocentric lunar libration was L = +1.8290°, B = -0.0997°, R = 354022.032 km.

It was slightly easier to time the disappearance of the photospheric continuum than the reappearance. As we can judge from Figure 5, the disappearance of the photospheric continuum at 2nd contact occurred a little faster than its reappearance at 3rd contact.

These are the contact times that we recorded, thanks to the UTC Event Timer:

C2 = 18:39:06.6 UTC
C3 = 18:39:20.3 UTC
Duration = 13.7 s

These experimental contact times can be compared with the contact time predictions by the various online sources, shown in Table 1.

Source	C2 (UTC)	C3 (UTC)	Duration (s)
timeanddate.com	13:38:55	13:40:00	65
eclipse2024.org (#1)	13:38:56	13:39:58	62
xjubier.free.fr (#1)	13:38:59.5	13:39:56.9	57.4
eclipse2024.org (#2)	13:38:56	13:39:32	36
xjubier.free.fr (#2)	13:39:00.8	13:39:25.3	24.5
besselianelements.com	13:39:06.1	13:39:19.0	12.9

Table 1. Contact times from some well-known sources of predictions.

The first prediction by eclipse2024.org is taken from the local circumstances calculator, while their second prediction is approximately gathered from the eclipse simulator. Also, the first prediction by xjubier.free.fr is read from the local circumstances displayed on the map, while its second prediction is computed by applying lunar limb corrections. The NASA predictions did not provide contact times, only a range of sophisticated eclipse maps, so we could not add it to the table. We can see that the closer the predicted northern limit is to the observation site (refer to Figure 1), the shorter the predicted duration of totality.

Of all the predictions, ours is the one that more closely reproduces the measured duration of totality and the experimental contact times. Considering that the manually timed contact times are affected by reaction time and other uncertainties, our predicted duration of totality is within the experimental uncertainty of that measurement (on the order of a couple of seconds) while all the others are substantially outside of it.

Note also that the uncertainty in the eclipse solar radius (±0.05") produces a variation in our predictions of only ±0.7 s (C2), ±1.1 s (C3), and ±1.8 s (duration). Thus, allowing for the substantial reaction time in the observed timing of C3 (likely much more than at C2), we can see that there's good overall agreement between our predictions and observations.

Further support for our predicted contact times is also provided by the QHY recording of the flash spectrum. Figure 6 shows frames bracketing the computed contact times. The reported time for each image corresponds with mid-exposure as recorded in the metadata of the FITS files.

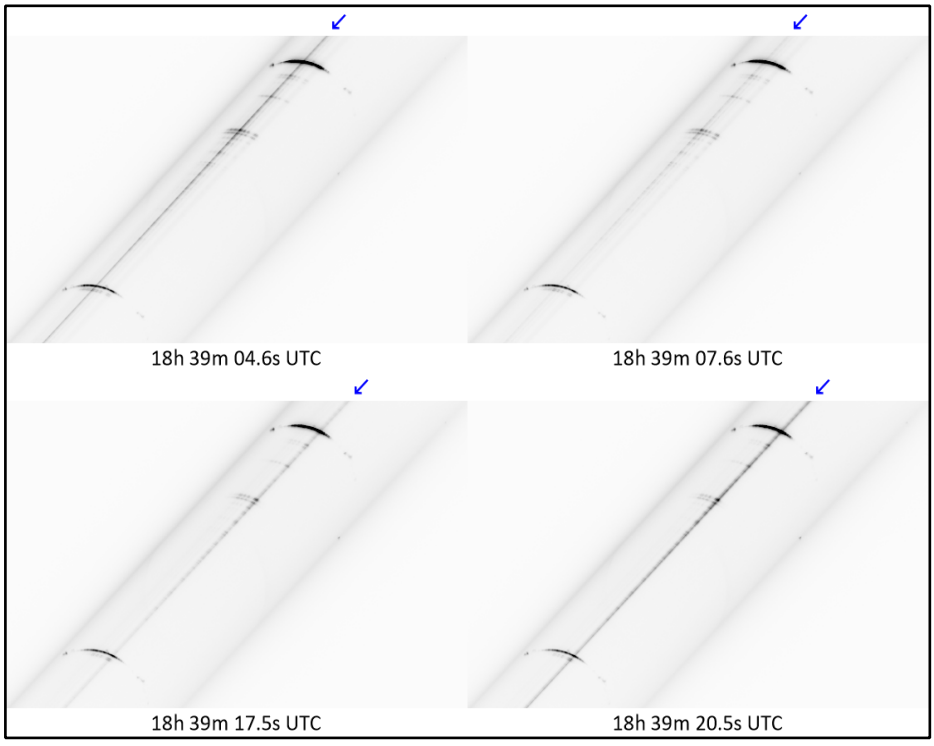

Figure 6. At top, two flash spectrum images spanning the time of 2nd contact computed by our model. Similarly, at bottom, spanning the predicted time of 3rd contact. The grayscale images have been reversed and sharpened to better highlight structure in the flash spectrum. The arrows indicate where the photospheric continuum disappears at 2nd contact (top) and reappears at 3rd contact (bottom). The transition is not sharp due to the presence of the mesosphere.

To estimate the occurrence of 2nd and 3rd contact, we need to look for the last and first traces of photospheric light. Its spectrum is continuous and it appears like a thin band of light in the flash spectrum. The light disappearing at the bottom of the lunar valley indicated by A in Figure 5, and reappearing at the bottom of the lunar valleys indicated by D in the same figure, are responsible for this spectrum. We also need to recall that the mesosphere, which lies just above the photosphere, is flooding the same lunar valleys at the times of 2nd and 3rd contact. As a result, considering that the mesosphere has a quasi-continuum spectrum, some fainter residual light will persist after C2 and also be present before C3. We cannot then expect a sharp disappearance and reappearance of the photospheric spectrum against an empty background.

Even if we cannot pinpoint the contact times with sub-second accuracy, the flash spectrum images support the fact that the photospheric continuum disappeared and reappeared sometime during the following UTC time windows:

18 h 39 m 04.6 s < C2 < 18 h 39 m 07.6 s
18 h 39 m 17.5 s < C3 < 18 h 39 m 20.5 s

This confirms that the manual contact timings are reliable.

Even though it is not the main emphasis of this report, the manual contact times collected at Stephenville also allows us to estimate an approximate value of the eclipse solar radius. Figure 7 shows the dependency of the contact times on the eclipse solar radius. Computations are based on our eclipse computational model. The blue and red lines display subtle slope changes due to the complexity of the lunar limb topography. Also displayed with dashed lines are the manually timed contact times.

Due to reaction time, second and third contact might have happened slightly earlier than measured. Even considering that the measured contact times are affected by 1-2 seconds of uncertainty, the experimental evidence supports the eclipse solar radius to be in the range:

959.9" < $S_\odot$ < 960.0"

This range is in line with eclipse solar radius estimations from the recent past.

To conclude this discussion, as most eclipse observers headed for locations near the centreline, we report in Table 2 the totality durations computed by the eclipse models listed in Table 1, this time for a site on the centreline experiencing maximum eclipse at the same time as Stephenville. This is the same location underlying the computations for Figure 2b.

We might expect, in light of what we gleaned from Figure 2, that the differences will be far smaller than ones seen near the umbral shadow path edge. This is indeed the case but even on the centreline differences around 1-2 s are still present. All other models predict totality durations longer than ours, by more than one second, noting also that the eclipse solar radius uncertainty (±0.05") translates to an uncertainty of only ±0.3 s in the duration.

Source	Duration
timeanddate.com	4 m 25 s
eclipse2024.org (#1)	4 m 24 s
xjubier.free.fr (#1)	4 m 23.9 s
eclipse2024.org (#2)	~4 m 25 s
xjubier.free.fr (#2)	4 m 23.8 s
besselianelements.com	4 m 22.5 s

Table 2. Centreline totality durations from some well-known sources of predictions.

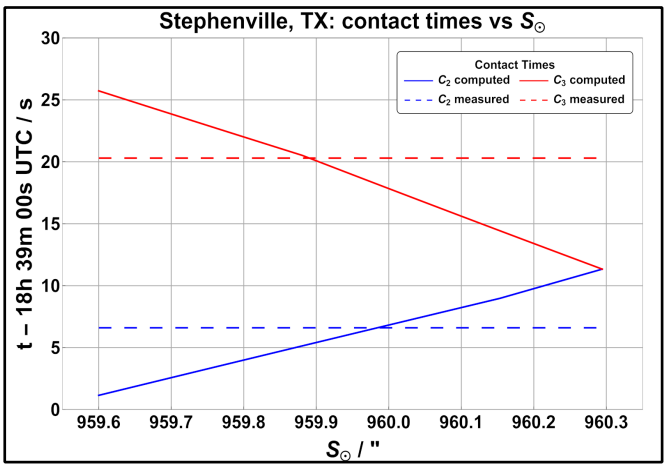

Figure 7. Dependence of the time of 2nd and 3rd contact on the value of the eclipse solar radius for Stephenville. Data sampling interval = 0.02". Also displayed are the measured contact times.

Other Edge Observations

Many of the TSE2024 reports we found online described observations of totality from locations around the centreline. But a precious few reported observations from near the eclipse limits. In light of what we have assessed so far about eclipse maps accuracy, we examine two of these reports to see how they fit in with our results. Although the observations are mainly qualitative in nature, we think their analysis is a good demonstration of how accurate eclipse predictions can help us interpret personal accounts of the eclipse experience from the edge.

Site #1: Gunter, Texas, USA

Jaime Zapata Suárez from Riobamba, Ecuador observed TSE2024 from Gunter. We learnt about this observation from the Solar Eclipse Chasers Facebook webpage [8]. The WGS84 coordinates of the observing location in Gunter City Park were:

λ = 96° 44′ 43.2" W
φ = 33° 26′ 39.8" N
h = 185 m

Figure 8 shows the observer's location in relation to the same eclipse limit predictions considered previously. Very strikingly, Jaime's location is just outside our predicted northern limit but inside all other predicted limits.

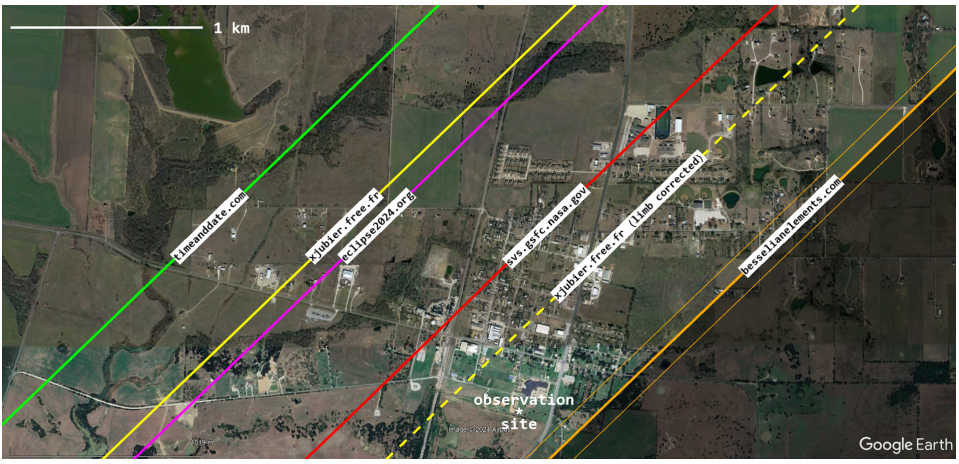

Figure 8. Comparison of various online predictions of the eclipse northern limit at Gunter, TX. Also displayed is the location of the observation site. (Map: Google Earth)

Jaime reports that the sky was clear over Gunter at eclipse time. Moreover, he describes that the ambient light noticeably dropped for several tens of seconds around maximum eclipse and the corona briefly became visible, albeit faintly. Jaime is an accomplished astrophotographer and he captured a sequence of unfiltered, high-resolution, eclipse images around maximum eclipse, some of which are shown in Figure 9. The four images cover a period of 16 seconds.

In the context of assessing the accuracy of eclipse maps, the main observation to be gleaned from these images is that Baily's beads never disappeared.

As highlighted previously, it is indeed challenging to time accurately the disappearance and reappearance of the photosphere. But our concern here is not with the timings themselves but with the fact that in all images we can see beads of very bright light surrounded by fainter whitish light (of mesospheric origin) and by the pinkish-purple chromosphere. It would seem very unlikely that these bright beads of light have an origin from anything other than the photosphere.

Jaime's images support the observation that, as the beads around "second" contact were vanishing, the beads at "third" contact were already brightening. This is very likely a sign that the observing location was just outside the path of totality, making our northern limit prediction the only one compatible with the experimental data.

Further insights are found by examining Figure 10 showing the relative motion of the solar and lunar limbs. We have identified the lunar valleys responsible for the Baily's bead seen in the images and labelled them with corresponding letters in Figure 9 and Figure 10. The diagram again uses an eclipse solar radius of 959.95" and is based on our own computations. Around time T_0 the simulation predicts that the photosphere would be visible, albeit barely, simultaneously in two distinct sets of lunar valleys (C/D/E and F) that are separated by about 15 degrees. This qualitatively agrees with what is visible in the second image of Figure 9.

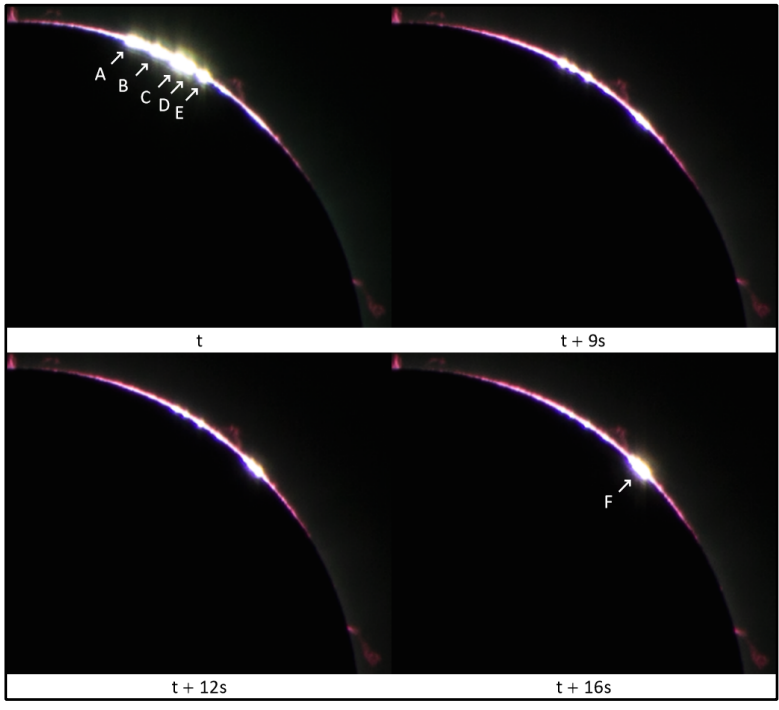

Figure 9. A sequence of unfiltered images of the eclipse as seen from Gunter, TX around the time of maximum eclipse. Refer to Figure 10 for the meaning of the letters A, B, C, D, E, and F, tracing Baily's beads back to specific valleys in the lunar limb profile. (Images: Jaime Zapata Suárez)

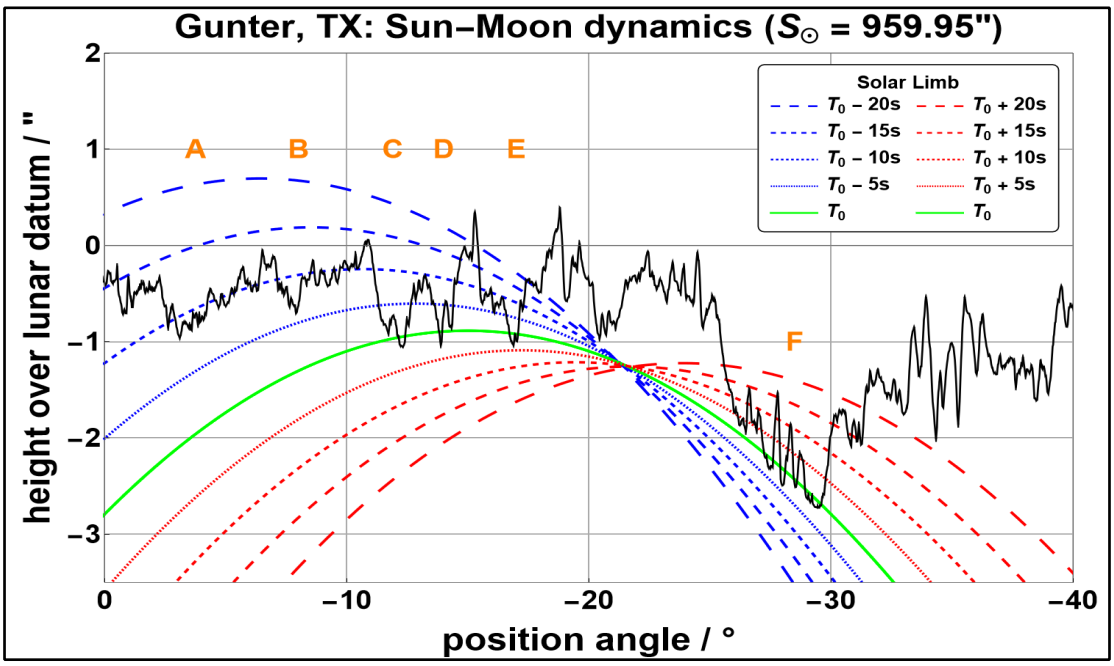

Figure 10. Relative motion of the solar limb with respect to the lunar limb (in black) for the observation site at Gunter. The lunar valleys marked with the letters A, B, C, D, E, and F generate corresponding features in the eclipse images presented in Figure 9. The reference time T_0 = 18:43:30 UTC, at which moment the apparent topocentric lunar libration was L = +1.7925°, B = -0.0996°, R = 354094.718 km.

Site #2: New Portland, Maine, USA

Jillian Culver from Truckee, California observed TSE2024 from New Portland under pristine skies. We also learnt about this observation from the *Solar Eclipse Chasers* Facebook webpage [9]. The WGS84 coordinates of the observing location, just to the west of the township, were:

λ = 70° 07′ 29.7" W
φ = 44° 52′ 53.1"
h = 164 m

Figure 11 shows this location in relation to the same eclipse limit predictions considered previously. The observation site was close to the eclipse southern limit, south of some of the predicted limits and north of most others.

Jillian's description of her eclipse experience is utterly fascinating. She describes the ambient light decreasing substantially, ushering in a period of semi-darkness for about 40-45 seconds.

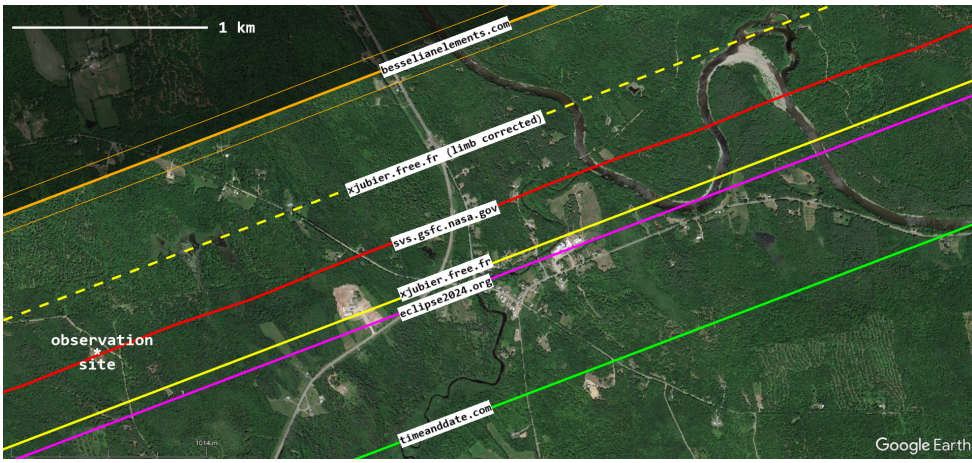

Figure 11. Comparison of various online predictions of the eclipse northern limit at New Portland, ME. Also displayed is the location of the observation site. (Map: Google Earth)

The full corona became visible while at the same time some easily noticeable Baily's beads were observable along the lunar rim. These beads seemed to "migrate" some distance along the lunar limb before the ambient light increased again and the corona vanished from view. Jillian also reports visibility of shadow bands on the ground.

Figure 12 shows three images taken with a smartphone by Jillian and depicting the first and the last diamond rings bracketing maximum eclipse. Around 50 seconds separate the first and the last image. The continuous presence of Baily's beads and Jillian's description confirms that the observation site was outside of totality by at least several hundred metres.

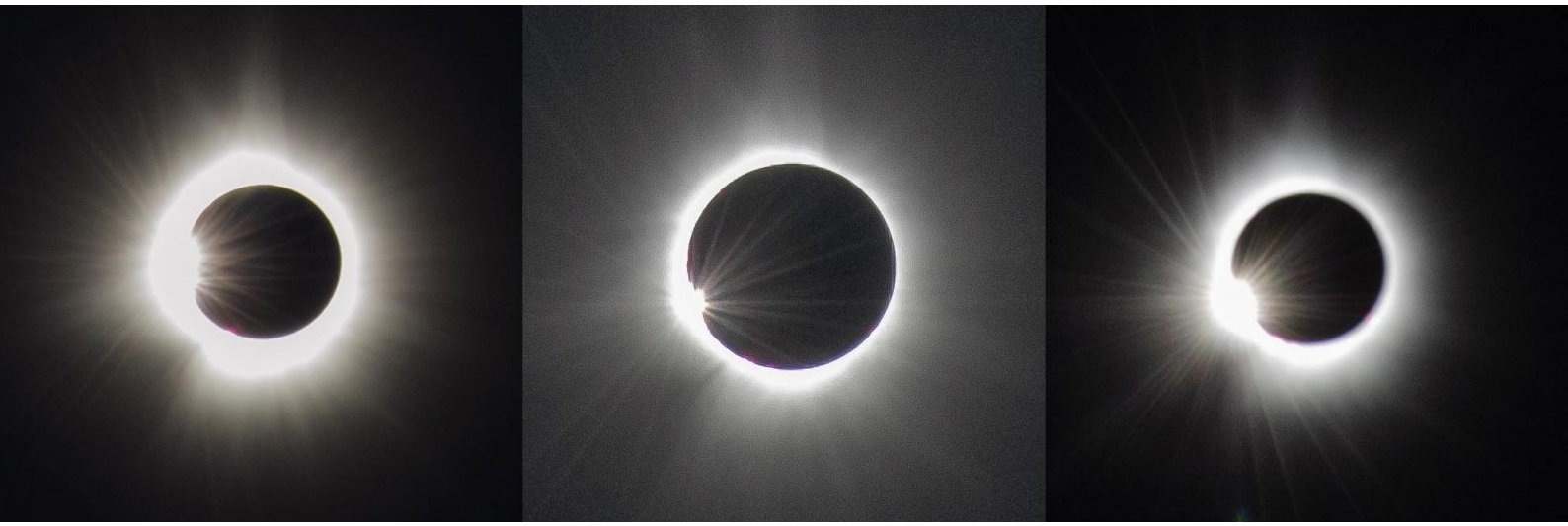

Figure 12. Sequence of images depicting the appearance of the eclipse around maximum eclipse as seen from New Portland, ME. (Images: Jillian Culver)

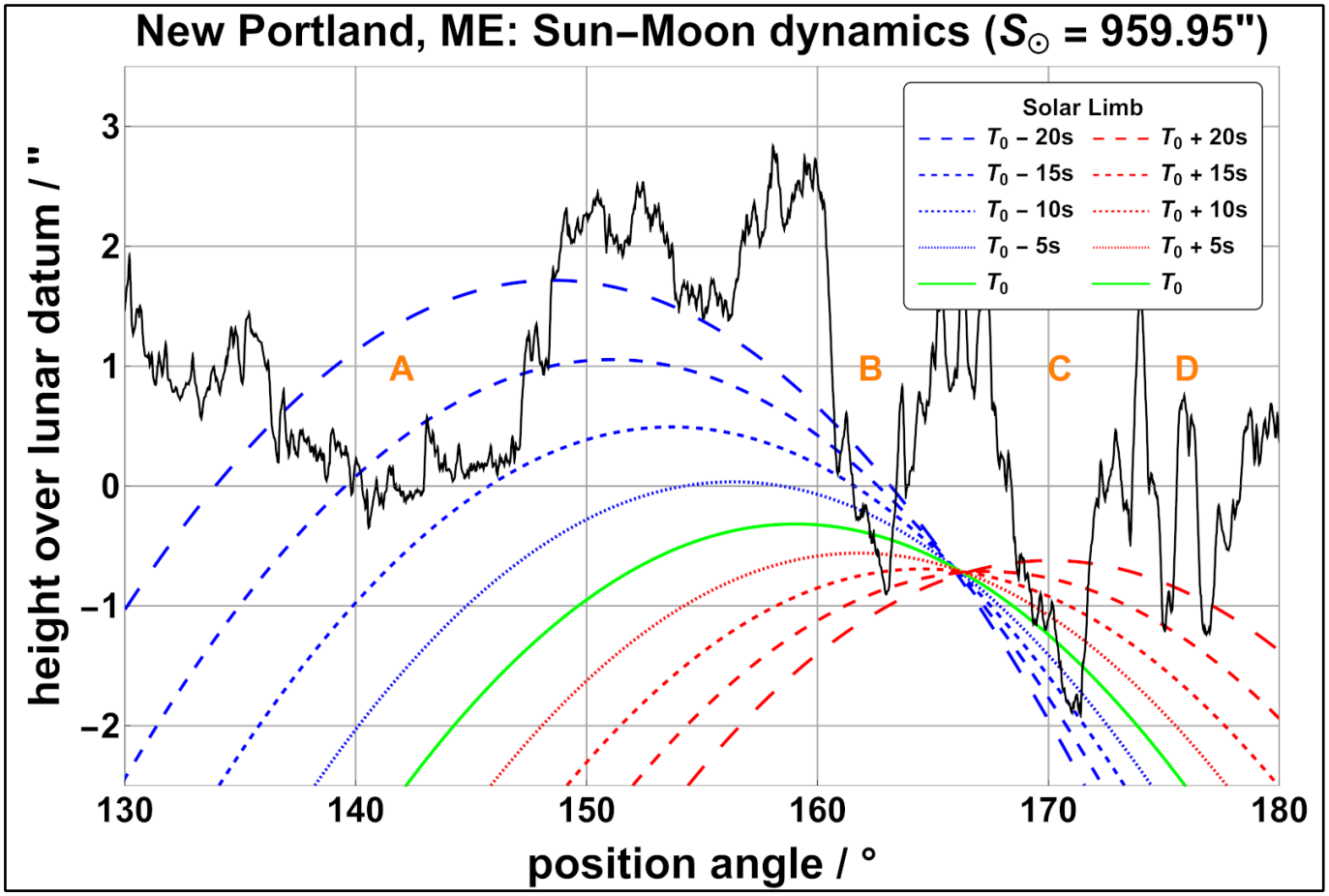

Figure 13. Relative motion of the solar limb with respect to the lunar limb (in black) for the observation site near New Portland. The lunar valleys marked with the letters A, B, C, and D explain features of this observation. The reference time T_0 = 19:31:05 UTC, at which moment the apparent topocentric lunar libration was L = +1.3798°, B = -0.1274°, R = 355950.193 km.

More insights are found by examining Figure 13 which shows the relative motion of the solar and lunar limbs. The first diamond ring is produced by the wide lunar valley marked with A. By about 10 seconds before T_0 only two small Baily's beads are left, generated by the lunar valleys marked with B and C. For the next 35 seconds, till T_0+15, these two inconspicuous Baily's beads are continuously visible, one shrinking and the other one expanding. During this period ambient light is likely to have dimmed sufficiently for the outer corona to become visible. The simulation very nicely reproduces Jillian's description.

Conclusion

In the lead up to TSE2024 we published an eclipse path map prediction based on our technically rigorous computational model. Based on experimental data collected during the eclipse from various locations very close to the eclipse path edge, these predictions have been shown to reproduce the umbral path limits and contact times more accurately than any other available online eclipse maps. It was shown that accounting for both the lunar and terrestrial topography, using an improved value for the eclipse solar radius, and utilising robust ephemeris computations, are crucial in predicting eclipse limits within 100-200 m from the real ones on the ground.

We would also like to note in passing that the experience of eclipse observers located marginally outside the umbral path limits is just as interesting and exciting as being inside the path, whether marginally or otherwise. To maximise the duration of eclipse transient effects and to have a prolonged view of the flash spectrum, we strongly recommend the path limits as the place to be during future total solar eclipses. And we invite eclipse observers in those locations, and also deeper inside the totality band, to consider gathering time-stamped flash spectrum data to contribute to this field of research.

Acknowledgements

We would like to express our deepest gratitude to Jillian Culver and Jaime Zapata Suárez who very kindly shared their eclipse locations, experience and images with us, providing invaluable observational data in addition to their Facebook posts. L.Q. would also like to thank Leonardo Pessi and Mascia Accordi for their assistance on eclipse day and for having been wonderful eclipse-chasing companions.

References

[1] Total Solar Eclipse on 8 Apr 2024: Path Map & Times, https://www.timeanddate.com/eclipse/map/2024-april-8

[2] Jubier, X., Total on Monday, April 8, 2024, http://xjubier.free.fr/en/site_pages/solar_eclipses/TSE_2024_GoogleMapFull.html

[3] McGlaun, D., Total Solar Eclipse of April 8, 2024, https://eclipse2024.org/eclipse_cities/statemap.php

[4] NASA, The 2023 and 2024 Solar Eclipses: Map and Data, https://svs.gsfc.nasa.gov/5073?linkId=204585126

[5] Irwin, J., Path of the 2024 April 8th Total Solar Eclipse, https://www.besselianelements.com/path-of-the-2024-april-8th-total-solar-eclipse/

[6] Quaglia, L. et al., Estimation of the Eclipse Solar Radius by Flash Spectrum Video Analysis, The Astrophysical Journal Supplement Series, vol. 256, no. 2 (2021), https://iopscience.iop.org/article/10.3847/1538-4365/ac1279

[7] Quaglia, L. et al., ATSE2023: Using Photodiode Loggers to Estimate the Eclipse Solar Radius, Journal for Occultation Astronomy, vol. 13, no. 4 (2023), https://iota-es.de/JOA/JOA2023_4.pdf

[8] https://www.facebook.com/story.php?id=202476246430394&story_fbid=7737510339593576

[9] https://www.facebook.com/story.php?id=174522229236725&story_fbid=7666800723342134

Journal for Occultation Astronomy

Observation of a Stellar Appulse of Comet C/2023 V1 (Lemmon) on 2024 August 27

Carlos Perelló · IOTA/ES · Agrupació Astronòmica de Sabadell · Sabadell · Spain · rigilk436@gmail.com
Antoni Selva · IOTA/ES · Agrupació Astronòmica de Sabadell · Sabadell · Spain · antoni.selva@gmail.com

ABSTRACT: Comet C/2023 V1 (Lemmon) attenuated the brightness of the star TYC 4233-01337-1 on 2024 August 27. The predicted occultation by the nucleus was not detected but, instead this, we recorded a clear drop in the light curve compatible with the presence of a dense coma that would have dropped down the magnitude of the star by 0.1 mag.

Introduction

The comet C/2023 V1 (Lemmon) was reported initially by *Steward Observatory*, Mt. Lemmon Station on 2023 November 2 [1]. There was previous observation reported to the MPC since 2022 September 23. The comet has a perihelion distance of 5.094 au and the perihelion will be reached on 2025 July 13 [1]. Currently the comet is 5.6 au from the Sun and 5.3 au from the Earth [2] (Figure 1). The orbit eccentricity (e) is 0.999 and the orbital period is at least 586.000 years [2]. Some other sources report e>1, then it is not clear if the comet will return.

Our observations were done from the *Agrupación Astronòmica de Sabadell Observatory*, Barcelona, Spain using the 50cm Newton telescope and a ZWO ASI432MM camera. Also, a GPS receiver ('mouse') was connected to synchronise the PC system time with GPS via USB and the images were captured using *SharpCap* [3] software in SER format.

You can find more data on the site *OccultWatcher Cloud* maintained by Hristo Pavlov [4], tag CometOcc at https://cloud.occultwatcher.net/event/1334-C2023V1-288159-651859-T01337-1.

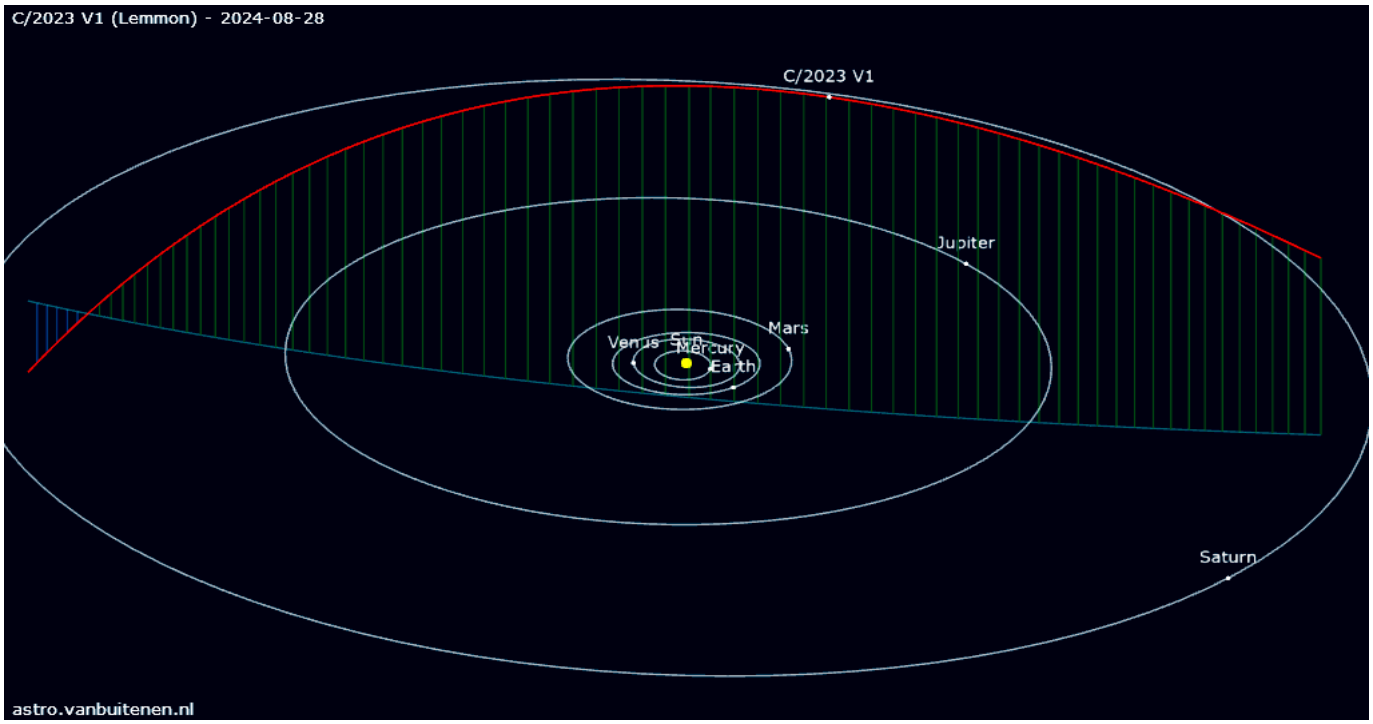

Figure 1. The orbit chart above shows the comet's path through the solar system and its position at the given date. Green and blue lines are shown perpendicular to the ecliptic plane: Green if the path is above the ecliptic plane, blue if it is below. (Screenshot: http://astro.vanbuitenen.nl/comet/2023V1 [5])

Observation

We prepared the observation like other stellar occultation of asteroid but we though in recording more time before and after the predicted central time (Figure 2) because we knew that some events can happen with the comets far away of the central predicted time.

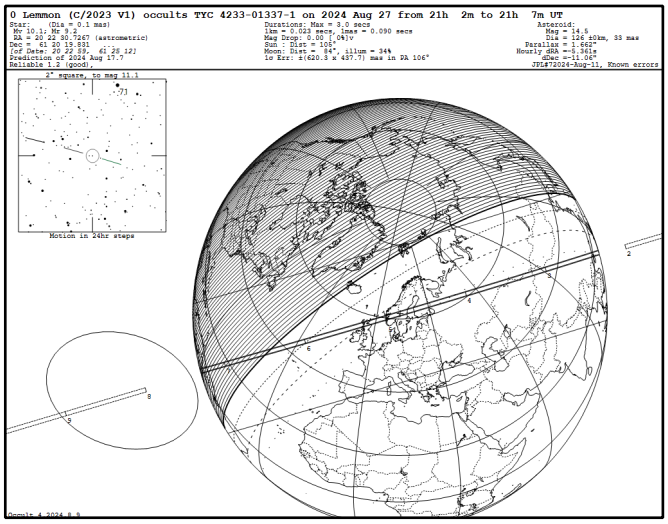

Figure 2. Path prediction based on data from Gaia EDR3 and JPL Horizons and computed with Occult V4.2024.8.9 [6].

When you prepare a comet occultation you should be prepared to recording a nucleus occultation (primary target and similar to the asteroid occultation, and less probable) and/or an attenuation of the light flux (secondary target and more similar to an exoplanet transit with progressive D and R).

As larger bits range camera is better for this kind of observations because the mag drop (in case of the secondary target above described) could be only a few tenths of magnitude. You should play before recording with the exposition time ensuring not saturate the target star (we use *Tangra's t*ool Target PSF Viewer), taking in to account choose too the shortest exposition to catch the nucleus occultation (if we were lucky).

Finally, we choose an exposition time of 0.04 s and recording ten minutes, unfortunately we start the recording 2 minutes late and decided to maintain the 10 minutes. There were no signals of any kind of occultation during the recording.

Our first visual impression was that the star did not disappear, but after the analysis we saw something in the light curve.

Observation Analysis

The light curve shows a drop of 0.1 magnitudes in a large period; about 20 seconds and shifted, approximately, 3 m 29 s after the predicted central time (Figures 3, 4).

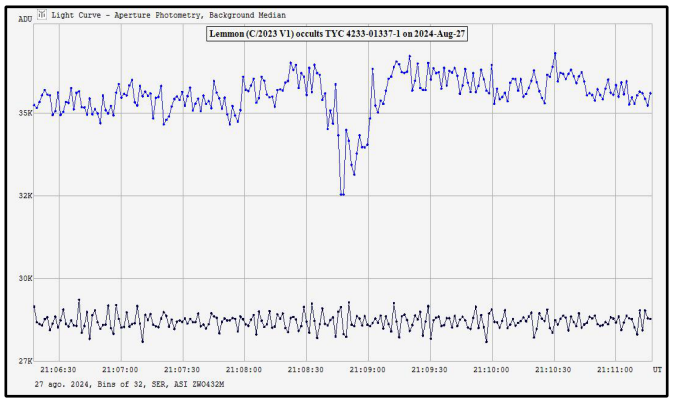

Figure 4. A normalised and binned chart of the light curve and zoomed in the area of the drop made with Tangra v3.7 [7].

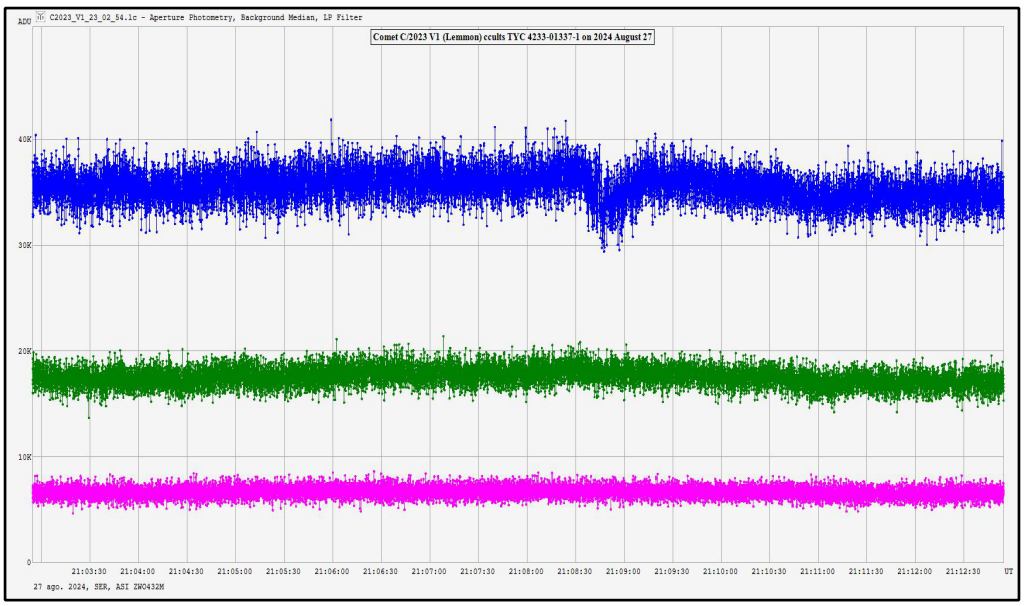

Figure 3. Light curve of the recording obtained with Tangra v3.7 [7]. The target star is in blue colour.

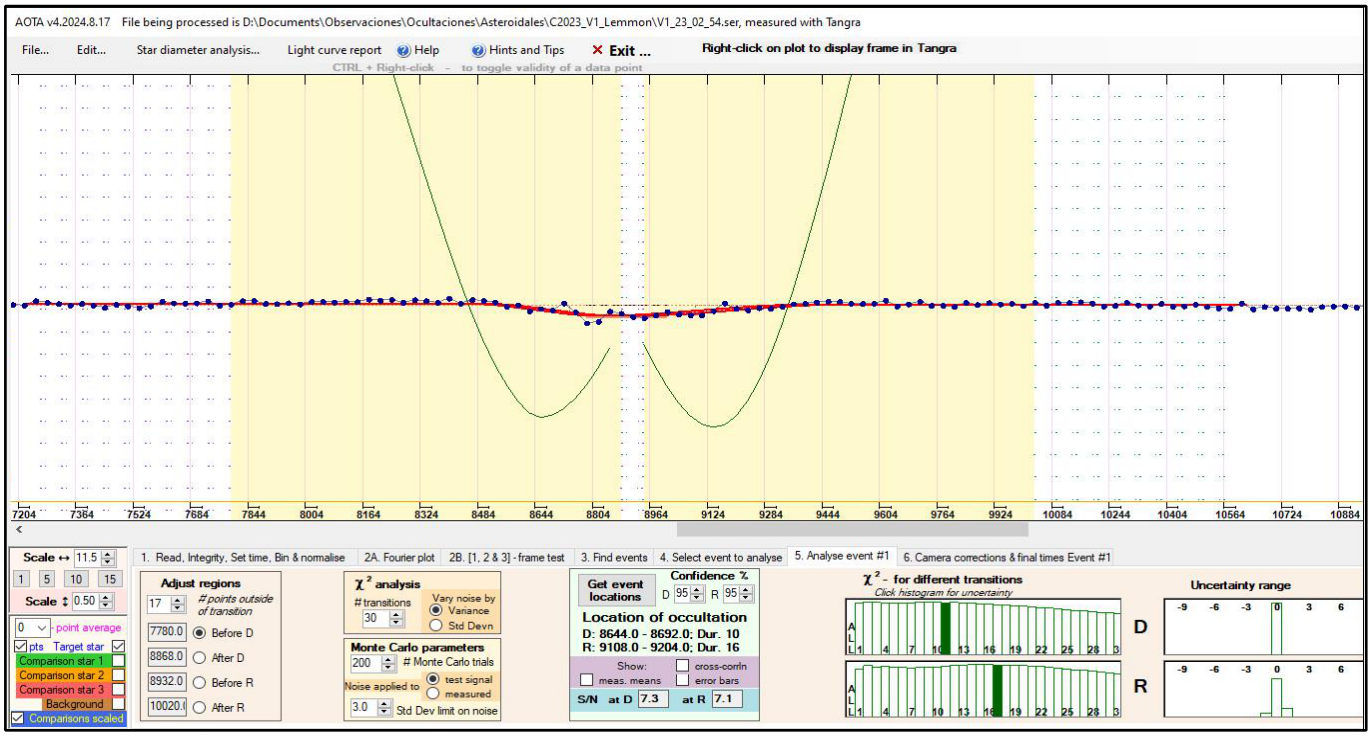

Figure 5. The lightcurve from Tangra analysed with AOTA [6]. See the different transitions of D and R in χ^2 histograms.

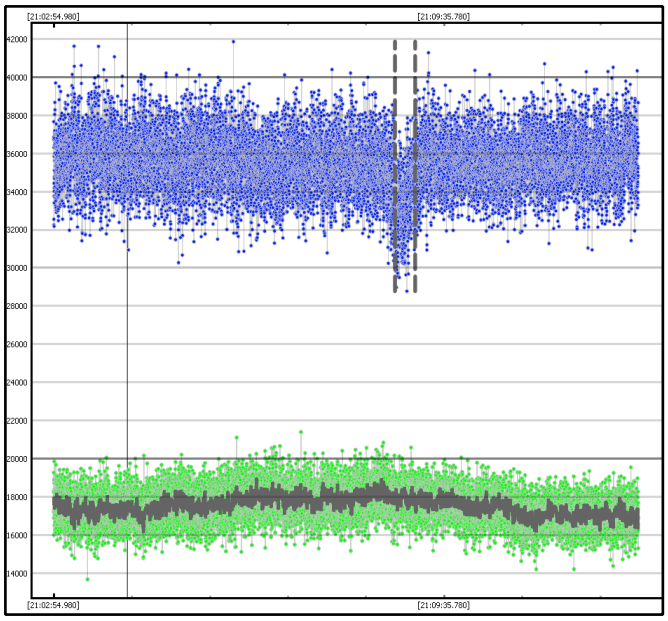

Figure 6. Light curve of the recording obtained with PyOTE 5.5.2 [8]. The target star is in blue colour.

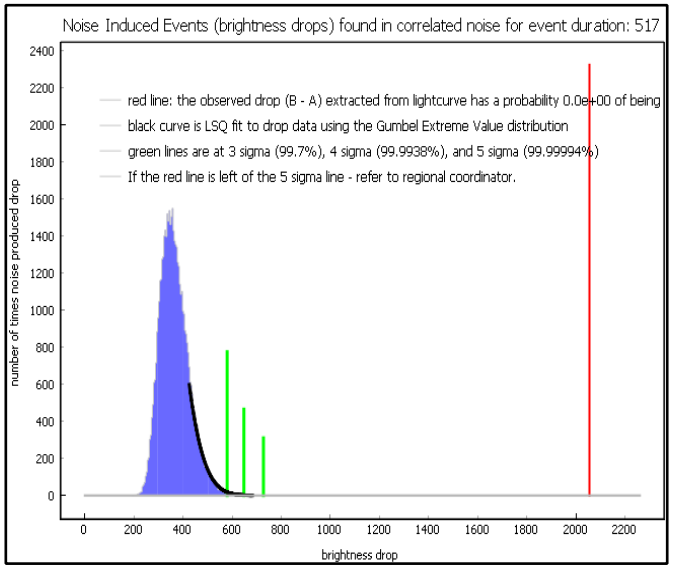

Figure 7. Noise induced events (brightness drops) found in correlated noise for event duration: 517. Obtained with PyOTE 5.5.2 [8].

Results

The drop recorded seems to be asymmetric, because the disappearance falls faster than reappearance. We believe that recover the normal light flux is slower than the drop down. May be that could be explained for the asymmetry of the, we guess, the comet coma as we see in a lot of images of comets where the nucleus is not in the centre (Figure 8).

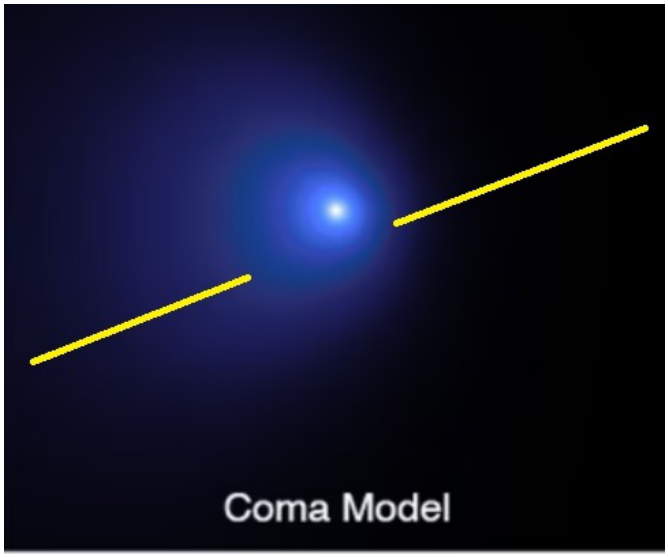

Figure 8. Coma model extracted from the Hubble Site [9] (NASA) used to isolated the nucleus of Comet C/2014 UN271 (Bernardinelli-Bernstein). The yellow line is a hypothetic chord that explain the asymmetry of D and R.

Analysing the recording with *Tangra* and *AOTA* we obtained an event duration (or duration of the light drop) of 19.6 seconds (Figure 5) while using *PyOTE* we obtained 20.7 seconds (Figures 6, 7), respectively. The measured magnitude drop is ~0.1 mag.

The measured length of a hypothetical coma chord would be between 823 km and 869 km taking into account the times of disappearance and reappearance are times in the middle of that events. Our chord was at 1765 km out of the predicted central path, in the limit of the 1 sigma zone.

The assumption that the drop recorded could be by the comet's coma is only an assumption; the most likely explanation is that the light drop was caused by a dense part of the (inner) coma.

Acknowledgements

The authors have made use of data from JPL Horizons provided by the Solar System Dynamics Group of the Jet Propulsion Laboratory and of data from the European Space Agency (ESA) mission *Gaia* (https://www.cosmos.esa.int/gaia), processed by the Gaia Data Processing and Analysis Consortium (DPAC, https://www.cosmos.esa.int/web/gaia/dpac/consortium). Funding for the DPAC has been provided by national institutions, in particular the institutions participating in the Gaia Multilateral Agreement.

References

[1] Minor Planet Center, https://minorplanetcenter.net
[2] Jet Propulsion Laboratory, Small Body Database Lookup, https://ssd.jpl.nasa.gov/tools/sbdb_lookup.html#/
[3] Glover, R., SharpCap software, https://www.sharpcap.co.uk/
[4] Pavlov, H., OccultWatcher Cloud, https://cloud.occultwatcher.net/
[5] van Buitenen, G., astro.vanbuitenen.nl, http://astro.vanbuitenen.nl
[6] Herald, D., Occult and AOTA software http://www.lunar-occultations.com/iota/occult4.htm
[7] Pavlov, H., Tangra software, http://www.hristopavlov.net/Tangra3/
[8] Anderson, B., PyOTE software https://occultations.org/observing/software/pymovie/
[9] NASA Hubble Space Telescope, https://hubblesite.org/

50 Years Ago – Graze Site Survey with Images from Outer Space

From *Occultation Newsletter* Vol. 1 No. 2:

SATELLITE AND AIRCRAFT PHOTOS
FOR RECONNAISSANCE USE

We have received a note from Thomas H. Campbell, Jr., further annotated by David W. Dunham. Mr. Campbell writes:

ERTS I Satellite, Skylab, Apollo, and Gemini, and aerial photos are available to the public. These high-resolution photos can be ordered for almost any area and scale, in black & white or color composites. These photos are highly useful to aid in scouting for a graze site. Since most topographic maps are old editions, they don't show new developments that might make a site unfavorable. For more details, write to Miss Frederika A. Simon; EROS Data Center; 10th & Dakota Ave.; Sioux Falls, SD 57198. Enclose $1.25 for standard U.S. catalog. Tell her your application for the photos, and you will be assigned a reference number for all future correspondence.

Dr. Dunham adds:

Detailed aerial photography is often available via U.S.G.S., which may be more recent than available maps, but probably not as recent as satellite photography, whose scale generally precludes accurate positioning.

More exiting stories from the past – ***The Occultation Newsletter Heritage Project***
https://www.iota-es.de/on_heritage.html

Journal for Occultation Astronomy

Stroboscopic Method for Verification and Adjustment of the Timestamp in Occultations

Javier de Elías · Agrupación Astronómica de Madrid (AAM) · Madrid · Spain · javierdeelias@gmail.com

ABSTRACT: This article shows a method for determining the timestamp accuracy of astronomical image captures. The method analyses the deviation between the timestamp associated with the images and the time given by a GPS PPS signal, achieving a sub-millisecond accuracy. The method has also been used to characterise the delays introduced by the readout time per line in most CMOS cameras due to the rolling shutter, which means that the position of the object to be measured in the image must be considered in order to determine the correct timestamp. By applying the method, we can characterise which offset to apply to our occultations and improve the accuracy of our measurements.

Introduction

Certain astronomical observations require a precise timestamp to be associated with them, such as the photometry of occulta tions, whether of stars by the moon or by asteroids. For some measurements, for example, when dealing with fast asteroids, it may be necessary to have an accuracy of better than one millisecond at the timestamp [1].

Basically, there are two options to mark the timestamp in each image: either the camera itself can do it, as it has an integrated GPS, e.g. QHY174M-GPS [2], or the camera control program will do it from the computer time, once the image has been received. In the first case, very precise timestamps are obtained, but in the case of cameras without GPS, important errors can be made, for example due to the time synchronisation method of the computer or the download time of the image from the camera to the computer. A special case is the delay introduced by CMOS sensors with rolling shutter in which the position of the object to be measured in the image must be considered and a correction related to the readout time per line has to be applied. It is precisely the presence of these errors, which can be tens of milliseconds, that justifies the need for a verification and correction method such as the one described in this article.

One of the most used time references today is the PPS (Pulse Per Second) signal obtained from the GPS (Global Positioning System) signal. This time reference is highly accurate, in the order of microseconds [3] and can serve as the basis for the generation of light pulses with very precise timing. One example is the SEXTA (Southern EXposure Timing Array) device [4] which uses a panel of LEDs that are activated sequentially so that when an image is recorded, the last LED to come on allows the time to be determined with an accuracy of 2 ms. Another option is the NEXTA (New EXposure Timing Analyser) device [5] which also uses LEDs but implements the improvement of encoding the time with an accuracy of 0.1 ms. Both devices have the disadvantage that they require focusing of the image of the LEDs on the sensor, so they are a good option to verify the precision of the setup, but it is complicated and impractical to use them to know the precision at the moment of the astronomical observation, since it would be necessary to point the panel of LEDs and adapt the focus, or use mirrors and optical elements to avoid having to manipulate the telescope in the moments before and after the astronomical observation. Another difficulty with these methods is that the precise verification process requires very short exposure times that are not possible with certain cameras.

The method described in this article also uses light pulses synchronised with the PPS signal, but with a simpler approach, as it uses a single LED and its use requires only placing the LED at the entrance of the telescope. Construction is much simpler, and there are even commercial devices that generate the necessary pulses. Moreover, it is not only a verification system, but can also be used just before and after the astronomical observation to check the deviation and correct the timestamp. The verification and correction method works with both fast and slow cameras and does not require short exposures to perform the verification. Sub-millisecond accuracy is achieved in the measurement of the deviation from the time reference set by a PPS signal.

Instrumentation and Method

Instrumentation

Two cameras, the ASI183MM Pro [6] and ASI120MM mini [7], have been used for testing the verification and correction method.

Both are monochrome cameras with CMOS sensors, but the method is also valid for cameras with CCD sensors. The ASI183MM Pro camera has a USB 3.0 interface, and the ASI120MM mini camera has a USB 2.0 interface, and they have been selected for

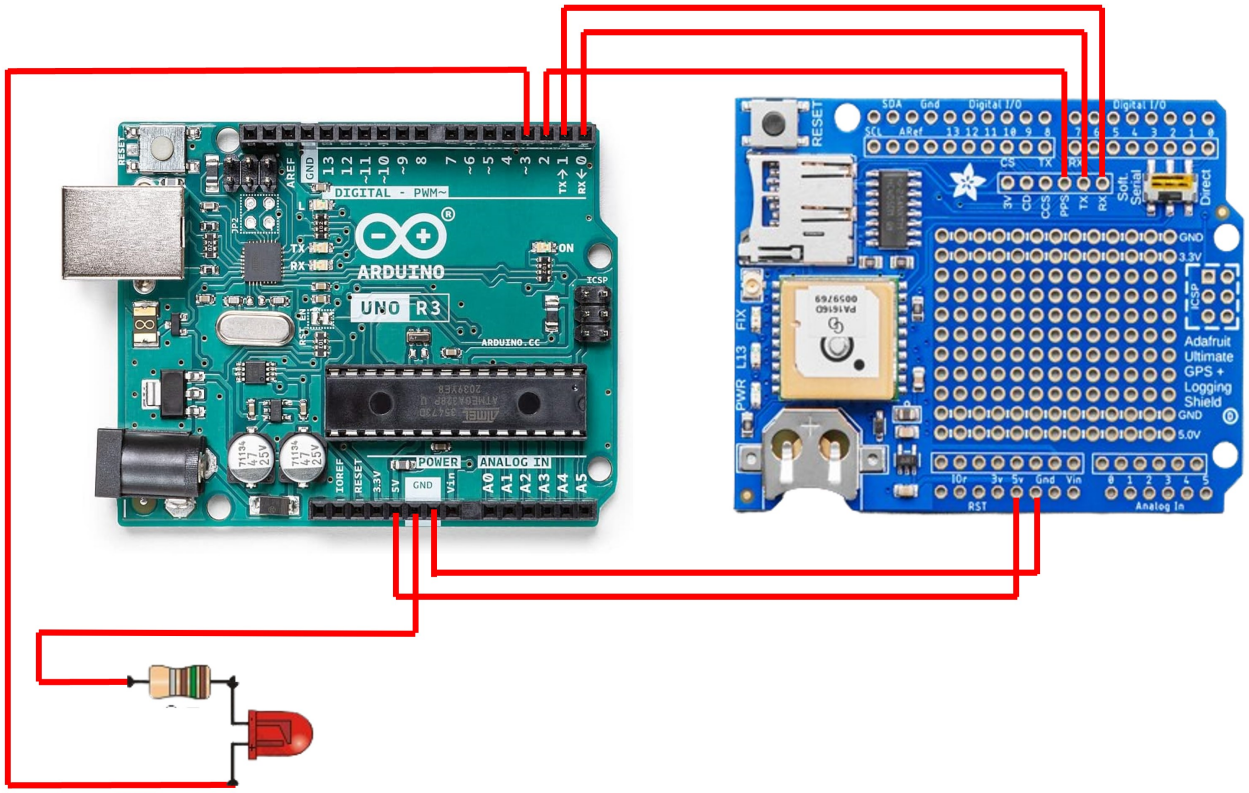

Figure 1. Connection diagram between the Arduino Uno controller and the Arduino Ultimate GPS Logger.

testing precisely because they are cameras with very different fps (frames per second).

For the generation of the light pulses synchronised with the GPS PPS, the following elements have been used:

- Adafruit Ultimate GPS Logger Shield [8]. This GPS receiver incorporates a PPS digital output necessary for the implementation of the method.

- Arduino Uno [9]. This micro controller receives the PPS pulse via a digital input and by programming (the source is included in the Annexes) an interrupt triggered by the rising edge of the PPS signal, a pulse of 500 ms duration is generated. Additionally, the RX and TX signals of the GPS receiver can be connected to receive NMEA 0183 type messages, but this is not necessary for the purpose of the application.

- An LED connected to a digital output of the Arduino controller with a resistor in series.

In practical applications of this system, the LED can be integrated into a translucent methacrylate ball and positioned at the entrance of the telescope. In the system tests no telescope was required and the LED was placed directly in front of the camera.

The device fabricated to generate the light pulses is shown in the Figure 2. To use the method described with this device, it is not necessary to implement the display and the box shown in the picture, it is sufficient to implement the schematic in Figure 1.

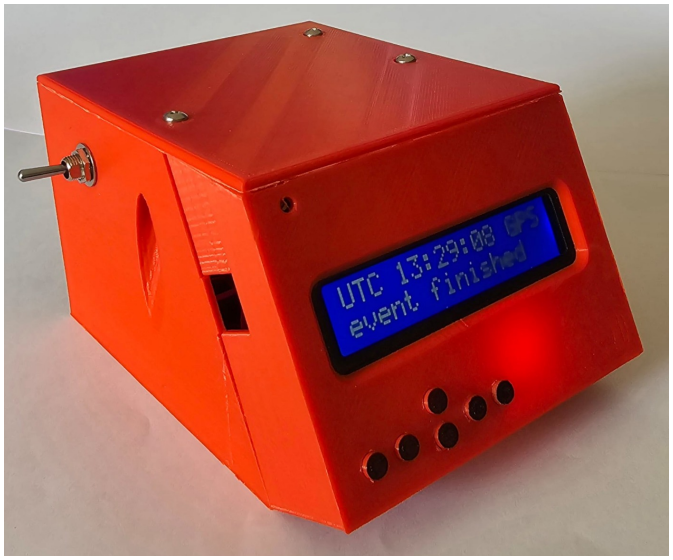

Figure 2. Device to generate light pulses.

Instead of manufacturing a device for the generation of the 500 ms pulse synchronised with PPS, it is possible to use other devices such as the GARMIN 18xLVC [10] which allows the pulse generation to be configured with its software.

Since the method aims to verify the timestamp accurately, it was decided to measure the delay that the assembly generates between the PPS pulse and the flash of light. For this measurement, a Thorlabs photometer model PDA10A [11] and a Keysight oscilloscope model DSOX3024T [12] were used, both with sufficient bandwidth to be able to carry out the measurement in the microsecond range. Two probes were used in the oscilloscope, one connected to the PPS output of the GPS and the other to the output of the photometer.

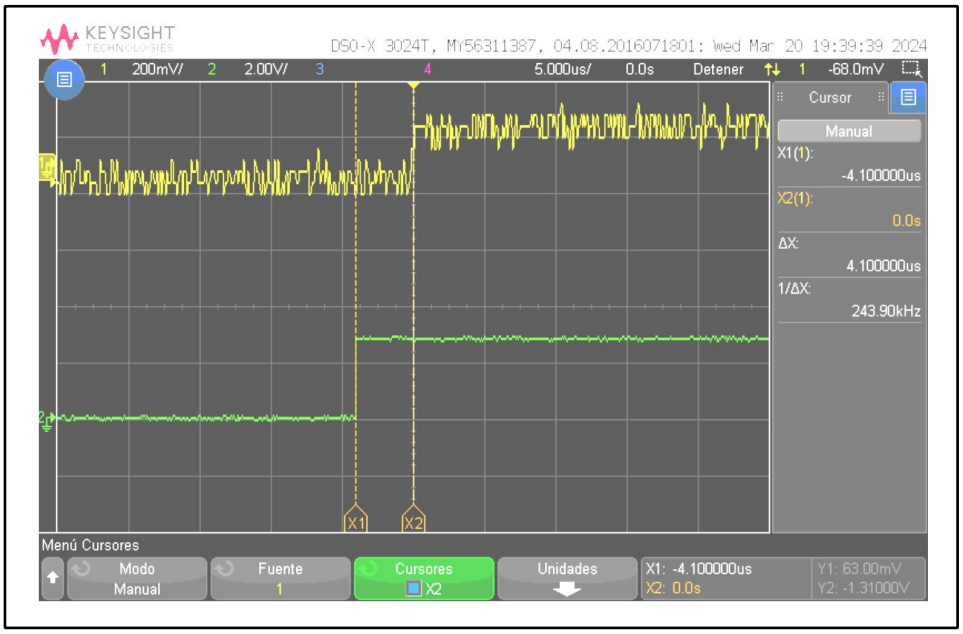

Figure 3. Measured delay between PPS signal and LED flashes. Green shows the pulse generated by the GPS and yellow shows the signal recorded by the photometer measuring the LED flashes.

Figure 3 shows the delay of approximately 4 microseconds, so it can be concluded that the setup provides a light pulse well synchronised with the PPS signal.

The computer used for testing is a laptop with 12th Gen Intel(R) Core (TM) i7-12700H 2.70 GHz processor and 32GB RAM, with *Windows 11*. For synchronisation the NTP service installed with the *Meinberg NTP* package [13] has been used. In the local network a Raspberry-based Stratum 1 time server with GPS PPS [14] has been used verifying throughout the tests that this host is selected for synchronisation and the PPS signal is in use.

The PC's time, synchronised with NTP and using the Stratum 1 server, will be used as a time reference to compare the timestamp measurements. The offset from the time server applied by the NTP service has been monitored during the test and is shown in Figure 4 for the interval in which the measurements were made with the camera ASI183MM Pro and Figure 5 with the camera ASI120MM mini. The average offset is 0.15 ms and 0.09 ms respectively, so during the tests the equipment was synchronised with an accuracy of better than 1 ms.

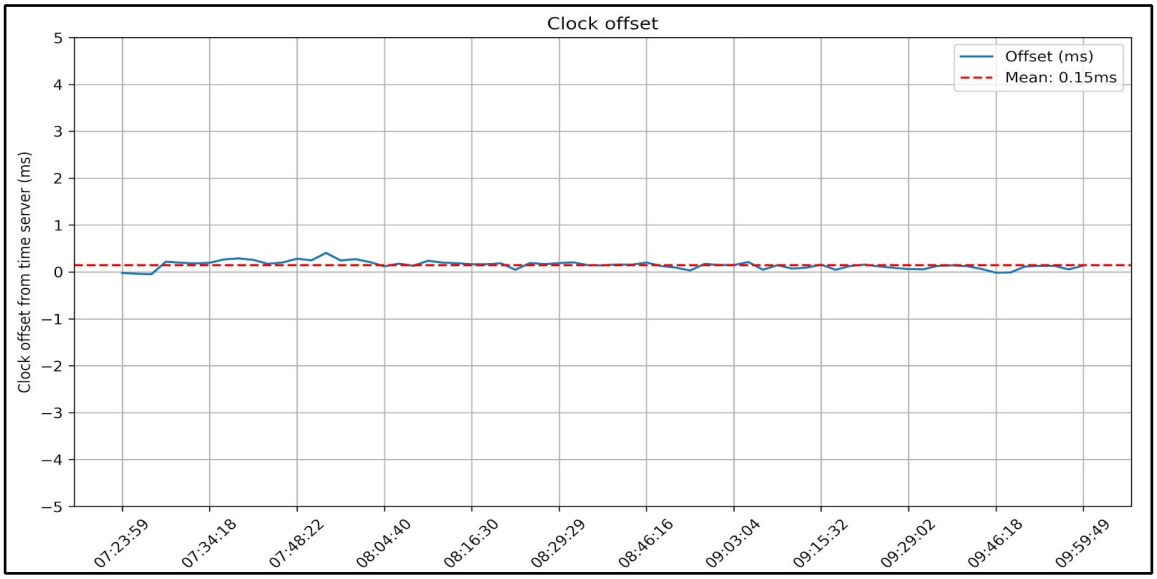

Figure 4. Offset from time server in the interval in which the tests with the camera ASI183MM Pro were carried out.

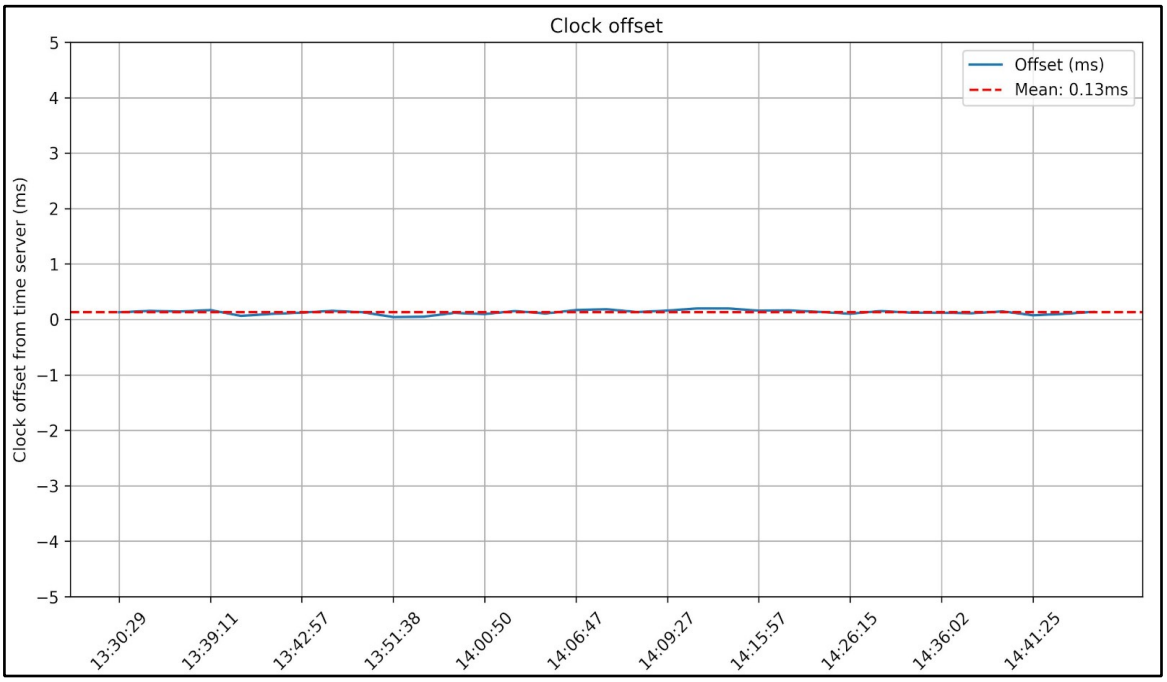

Figure 5. Offset from time server in the interval in which the tests with the camera ASI120MM mini were carried out.

The *SharpCap* software [15] in version V4.1.11824 was used to control and download the images. This software performs the time stamping of the images using the time of the computer as a reference when receiving the images and subtracting the exposure time. The tests were carried out by configuring *SharpCap* to generate a sequence of FITS files.

For the analysis of the generated images, the *Tangra* software [16] in its V3.7.5 version was used. This software allows the generation of a light curve in CSV format (comma separated values) from which the difference between the time according to the PPS signal and the timestamp of the images is calculated with the procedure explained in the following section. Another recommended tool for such an analysis is the software *PyMovie/PyOTE* [17].

Method

Principle of operation (stroboscopic effect)

The developed method consists of generating and recording light flashes with a duration of 500 ms, whose rising edge is synchronised with the PPS signal obtained by a GPS receiver. Using the setup described in the instrumentation section, the Arduino controller activates an output connected to an LED every time it detects the rising edge of the PPS signal. The LED therefore generates an illumination pattern so that every second the first half of 500 ms is on and the second half of 500 ms is off. The light signal thus described is recorded by the camera with an exposure time slightly longer than that of the light pulse. An exposure time of 505 ms, i.e. a time offset of 5 ms, has been selected to generate a stroboscopic effect.

The camera will start recording at an arbitrary time which, in general, will not be synchronised with the on/off pattern that occurs every 500 ms. It is precisely the difference between the flash duration and the exposure time that is decisive for the intensity level of each frame to vary from shot to shot. Figure 6 shows how this works.

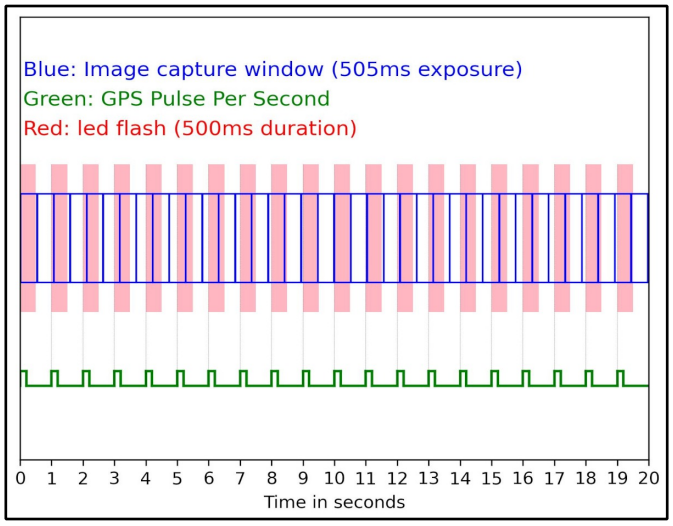

Figure 6. Principle of operation. The 5 ms offset is not scaled.

In the captured image sequence, the odd and even images are analysed independently, and it is observed that in each of them the average intensity will go up from a minimum in which the image coincides with the part of the second in which there is no flash, to a maximum in which the image coincides with the opposite case, that is, synchronised with the flash. The odd and even images are complementary, when one has a maximum, the

other has a minimum and the slopes of the curves showing the evolution of the intensity have opposite signs. As the time offset progresses during the capture, in the general case there will not be perfect synchronization at any time, but the method will allow the maximum and minimum to be calculated accurately.

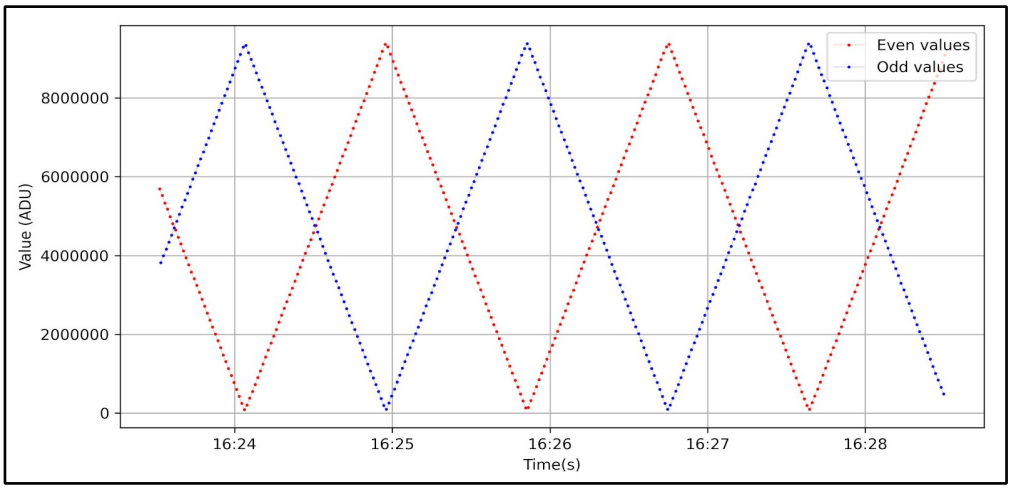

Figure 7. Example of a light curve obtained.

Figure 7 shows a typical light curve obtained by this method (the image is a result of the *Python* program described in this document), in which the light curves of the odd and even images have been differentiated. The curves will consist of straight sections as long as the LED intensity stays within the linearity zone of the sensor (no saturation). Both curves are treated identically in the processing, but independently of each other. The objective is to determine the maximum and minimum for each of the curves. We will see that each maximum or minimum allows us to calculate a deviation in the timestamp and then we will average all the calculated deviations.

To estimate the time between maxima or minima of an even or odd curve, we must take into account that for it to produce a maximum or minimum again, we have to generate a displacement of the observation window of 1 s. In the example given for an exposure duration of 505 ms, as each second produces a displacement of 10 ms (corresponding to 2 images), we need 1000/10=100 s to elapse. If the exposure time is 5 minutes, we will obtain 3 maximums and 3 minimums for the curve of even and the same for the curve of odd images, so we will be able to average with 12 measurements.

To accurately calculate the maxima and minima of the light curves, N points are determined on either side of each approximate maximum or minimum found. For each set of N points, a regression line is calculated, and the maximum or minimum is recorded as the intersection of the two lines.

The value of N, the number of points for the linear regressions, has been set to a minimum of 10 during the tests. The minimum of 10 means that in some cases the calculation cannot be performed (depending on the distance of the maximum or minimum from the beginning or end of the capture), so that the total number of values to be averaged in 5 minutes and with 505 ms exposure can sometimes be one or two units lower than 12. Although 5 minutes is considered an adequate interval to obtain sufficient measurements, it can be extended to obtain more measurements to improve accuracy.

Figures 8 and 9 (the images are a result of the *Python* program described in this document) show graphically the procedure of obtaining a maximum and a minimum respectively by calculating the intersection point.

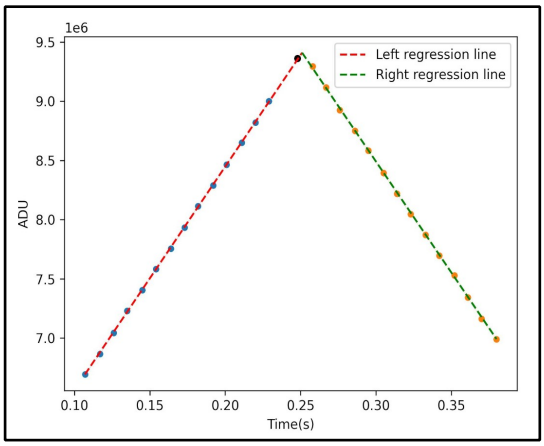

Figure 8. Obtaining a maximum as the intersection of the regression lines.

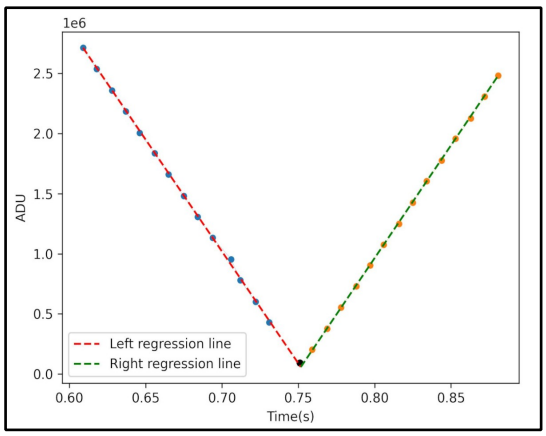

Figure 9. Obtaining a minimum as the intersection of the regression lines.

Light Curve and Processing

In the tests carried out, *SharpCap* has been configured to record a sequence of files in FITS format. The analysis has been carried out with the *Tangra* software, oriented to the processing of occultation captures. For this purpose, the "no tracking" mode was selected choosing an area near the centre of the image for the photometry and using only one aperture. Once the light curve is obtained, it will be exported to a csv file. The appearance of the light curve provided by *Tangra* may not show the pattern of maxima and minima as *Tangra* subtracts the background which will not be done when processing, as only the signal of the photometric circle will be used (the csv file generated by *Tangra* offers signal and background in differentiated columns).

The parameters in Figure 10 have been configured for reductions with *Tangra*.

The stroboscopic method generates maxima and minima of the light curve which in perfect synchronisation should coincide with the first half of the second (i.e. a timestamp value of the type xx.250 s) or the next half of the second (i.e. a timestamp value of the type xx.750 s). The deviation is measured by subtracting the value of the maximum or minimum of the time closest to xx.250 s or xx.750 s, i.e. we only subtract the milliseconds ignoring the seconds. This allows us to detect variations of at most 500 ms, so this method can only be applied for fine-tuned detections of timestamp deviations.

For the automatic analysis of the light curve, a *Python* program (Included in the Annexes) has been developed that separates the measurements into two dataframes: one for the even and one for the odd frames. For each dataframe, the maximum and minimum values are obtained and the regression lines around each value are calculated to obtain the time associated with the intersection of the lines. From the data obtained, the associated delay or advance in milliseconds is extracted and the mean is calculated, as well as the standard error.

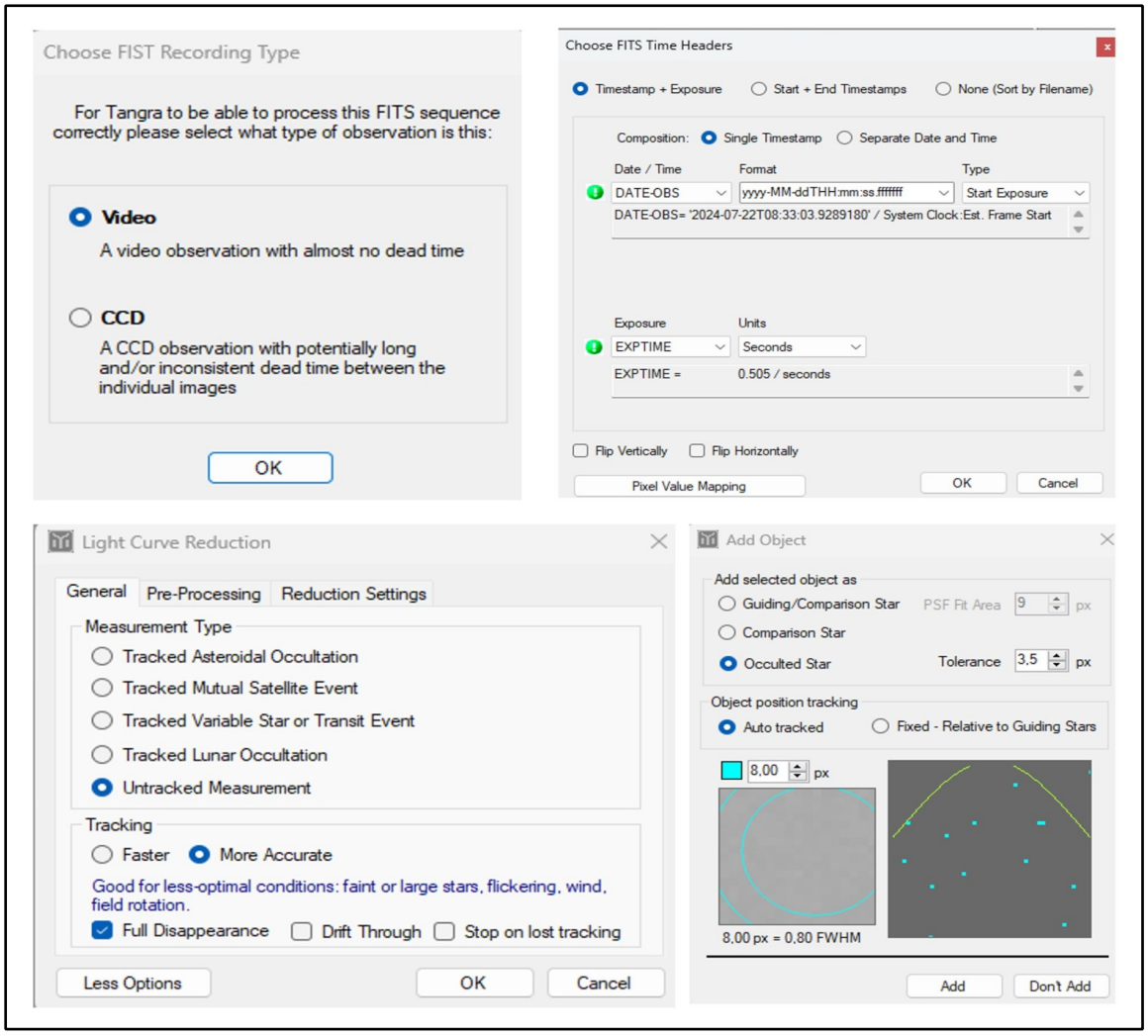

Figure 10. Screenshots to indicate the configuration used in Tangra.

Results

Accuracy of Time Stamp

Table 1 shows the results measured with the AS183MM Pro camera, with an exposure of 505 ms, binning 1×1, no gain, 5-minute image capture. All the recordings have been made with a frame size of only 32×32 in the centre of the image. The column samples indicate the total number of maxima and minima obtained and used to average the result and calculate the standard error between the samples. The mean of the measurement series is 0.48 ms, with a standard error (between the averages) of 17 µs. According to Figure 4, the average offset measured by the NTP during the tests was 0.15 ms, so we obtain a difference of 0.33 ms, which we will discuss in the next section.

Delay (ms)	Error (µs)	Samples
0.46	89	12
0.49	57	10
0.59	107	12
0.48	80	12
0.45	76	10
0.47	86	12
0.41	73	10
0.51	63	12
0.52	87	10
0.43	86	10

Table 1. Results with frame size (32×32), AS183MM camera, exposure 505 ms, duration each 5-minute measurement. Mean value of 0.48 ms, standard error of 17 µs.

Table 2 shows the results of a test under the same conditions but with the ASI120MM mini camera. According to Figure 5, the average offset measured by the NTP during the tests was 0.13 ms, so we obtain a difference of 1.2 ms, which we will discuss in the next section. There is an important difference between this result and that obtained for the ASI183MM camera which will also be explained also in the next section.

Delay (ms)	Error (µs)	Samples
1,20	61	10
0.92	136	12
1.06	34	10
1.05	47	10
1.11	51	10
1.07	46	10
1.26	82	10
1.27	53	12
1.09	44	10
1.27	69	10

Table 2. Results with frame size 32×32, AS1120MM minicamera, exposure 505 ms, duration each 5-minute measurement. Mean value of 1.33 ms, standard error of 51 µs.

Row Dependence of the Time Stamp in Sensors with Rolling Shutter

An interesting result of the tests with the stroboscopic method was the fact that measuring the timestamp in different rows for the same sequence of images generates different results. Figure 11 show the measured values in three different rows of the images: one as close as Tangra allows to the top edge, another in the centre of the image and the third at the top edge. With the camera ASI183MM Pro, an 800×600 ROI and a 1280×1024 ROI sequence were used. In both cases, a linear response with a slope of 0.0127 in one case, and 0.0126 in the other is observed. The explanation is simple: the time stamp of the image corresponds to what happens in the first row, while in the following rows what happens in the image takes places at a later time. The reason for this effect is the rolling shutter of the tested camera, i.e. the image picks up what happens in each row as the camera unloads the corresponding row from the sensor. According to this explanation, a timestamp must be associated with each row, which is the sum of the image timestamp (which can be associated with the first row) plus the readout time per row (sensor download time of a row) multiplied by the row number. In the tests carried out with the two ROI's indicated, the reading time per row is 12.7 µs and 12.6 µs (slope of the lines), so an approximate value of 13 µs is estimated.

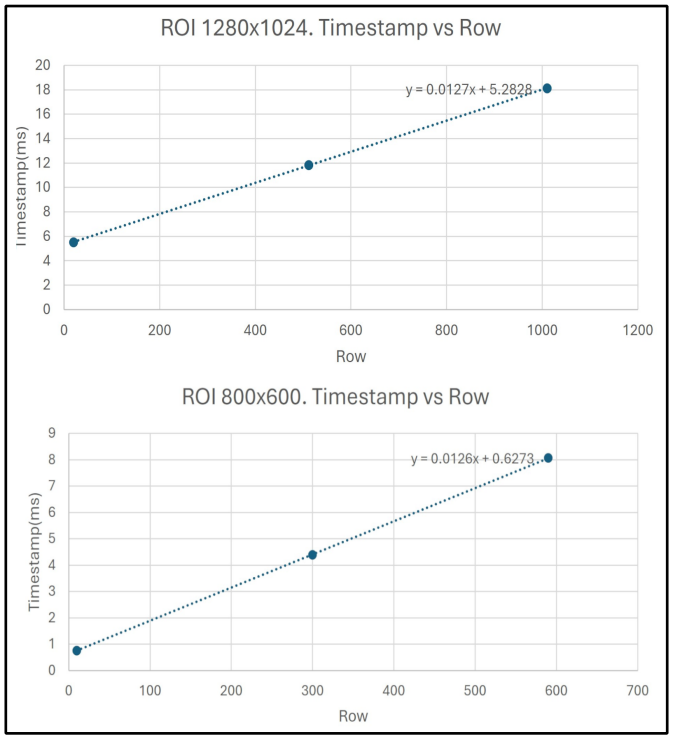

Figure 11. Timestamp measurements in different rows for two different ROIs, using the ASI183MM Pro camera.

To support this result, an additional experiment has been carried out, which also allows the readout time per row to be measured in a very simple way, albeit with somewhat less precision. The idea is to place a light source from the camera powered by AC power

source. For the test I used a Neon pilot. Simply capture an image (exposure time is not relevant), just be careful not to saturate, and measure the number of lines between two maxima. If we divide 100 ms (how long the Neon takes between two maxima) by the number of lines separating two consecutive maxima in the image we get the readout time. I have obtained a separation of 269 lines which gives a readout time of 13.3 µs, less than 1 µs difference with the value obtained with the stroboscopic method.

Figure 12. Image captured with Neon light and camera ASI183MM Pro.

The same tests have been carried out for the ASI120MM mini camera with a readout time of 66 µs.

Let us now return to the results obtained for the 32×32 ROIs. In the case of the ASI183 camera, the average result was 0.48 ms. If we subtract from this value the readout time corresponding to row 16 where the measurements were taken (centre of the image), we have 0.48-16*0.013=0.27 ms, when with the NTP we obtained an average time lag with respect to the server of 0.15 ms (Figure 4). In the case of the ASI120MM mini camera, the average result was 1.33 ms. If we subtract from this value the readout time corresponding to row 16 where the measurements were taken, we have 1.33-16*0.066=0.27 ms, and with NTP we obtained an average time offset of 0.13 ms (Figure 5).

In both cases, the difference between the measured time and the expected time according to the PC offset monitoring with the NTP service is of the order of 0.1 ms, a difference that can be attributed to both the processing of the cameras and the software downloading the camera images. This is, however, a very small time and within the sub-millisecond that I consider the stroboscopic method allows us to measure.

An additional test performed was to measure the timestamp of the central row of different ROIs. Table 3 shows the results. Without going into a detailed analysis that would require a deeper knowledge of how the camera firmware manages the timestamp, we can conclude some interesting results:

- The timestamp associated with the centre line of the image sequences increases as the row on which we measure increases.
- Up to an ROI of 320×240, the increase corresponds to the readout time quite well, but as the ROI size increases, the curve loses linearity and it is necessary to consider other additional factors to explain the higher timestamp, such as the download time between the camera and the PC.

ROI	Measured Row	Time (ms)
32×32	16	0.4271
48×64	32	0.6212
192×192	96	1.521
320×240	120	1.6693
496×350	175	2.6816
800×600	300	4.3892
1024×768	384	6.4449
1280×1024	512	11.8434
1600×1200	600	19.1985
1832×1836	918	34.8295

Table 3. Results in different rows, with ASI183MM Pro, exposure 505 ms, 5-minute measurement.

All measurements were made with gain and offset 0, 16-bit colour space and 1×1 binning. It has been found that the readout time per row does not vary if the binning, gain or offset are changed, but it does change if the colour space is changed: 16-bit gives twice the readout time per row as 8-bit. However, this may depend on the camera used and it is recommended to measure the readout time per row with the same configuration with which the occultations are going to be made.

Measurement of PC Time Drift

The stroboscopic method has also been used to measure the time drift of the PC when it deactivates the NTP synchronisation. To perform this test, the NTP service was forced to stop for one hour and the time stamp was measured with 5-minute series, using a 32×32 pixel ROI and the ASI183MM Pro camera. Figure 13 shows the result, which turns out to be very linear with a drift reaching 100 ms in one hour.

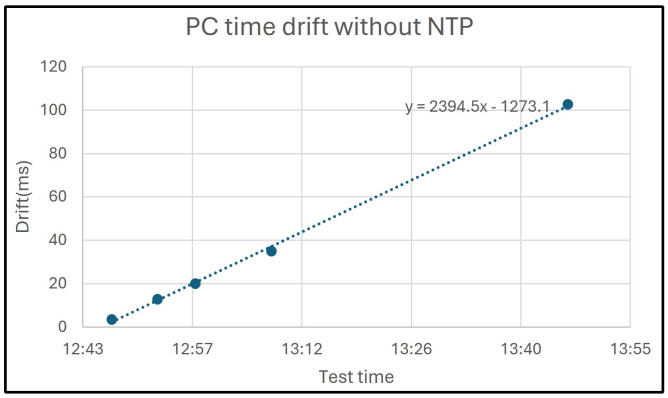

Figure 13. PC time drift when stopping NTP synchronisation.

This result highlights the importance of keeping the PC synchronised to obtain correct results in occultation measurements.

Discussion

Flash Pulse Duration and Offset Setting

In applying this method, a flash pulse of 500 ms duration and an observation window of 505 ms generates the stroboscopic effect. The question arises as to whether this is the correct selection and why.

Regarding the duration of the flashes, we studied the alternatives of 250 ms and 1000 ms. In the case of 250 ms, we would have to generate, between two rising edges of the PPS signal, a first 250 ms pulse, wait 250 ms, and generate another 250 ms pulse. This poses a technical problem in that the second 250 ms pulse cannot be triggered by an interrupt, so the high accuracy obtained from only 4-microsecond difference between the rising edge of the PPS signal and the light pulse cannot be guaranteed. In the case of 1000 ms pulses, the above-mentioned problem does not occur, because it is only necessary to prepare the code so that, with the interruption of the rising edge of the PPS, the pulse of 1 s is alternately activated or deactivated. However, this pulse of twice the duration does not bring any advantage, it only makes the time between maxima and minima longer and consequently the measurement procedure longer. Based on the above, it is considered that light pulses of 500 ms are the most suitable option.

Regarding the length of the observation window, we can consider options between 501 ms and 510 ms. In the case of 501 ms, the time between maxima or minima would be of the order of 8 minutes (1000/2 = 500 s) with up to 125 (500/4) points to define the regression line before and after a maximum and a minimum. In the case of 510 ms the time between minima or maxima would be 50 s and the number of points for each regression line would be only 12. For 501 ms, the time of 8 minutes is considered excessive to establish the total time of the video in order to have enough maxima and minima to allow averaging. On the other hand, at 510 ms the number of points for the regressions is too low. The 505 ms option is a suitable compromise, as it provides sufficient and well-sampled maxima and minima to obtain the regression lines in the 5-minute measurement.

Effect of the Rolling Shutter on the Time Stamp of the Measurements

Most CMOS cameras use a rolling shutter, which is an advantage as it increases the frame rate by not having to stop between exposures. But this way of reading implies that the different parts of the captured image correspond to different events in the time domain [18].

Suppose an image where the object to be measured is in the first row, the associated timestamp would be t1 (Figure 14), but if the centroid was in row 1000, the associated timestamp would be t1000. The difference between the two times is the readout time

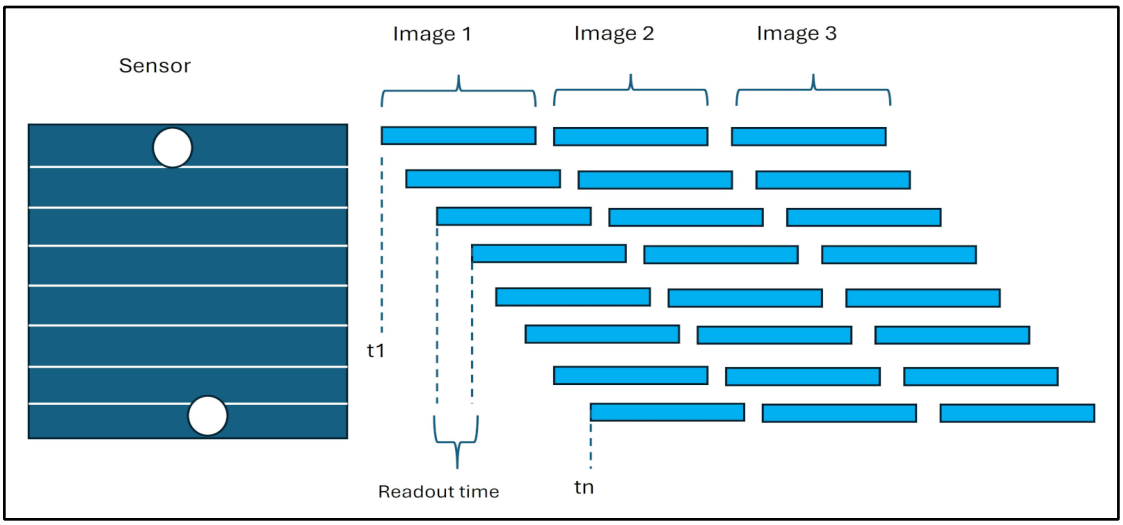

Figure 14. Rolling shutter. t1, tn refer to the text.

per row multiplied by the number of rows between the two measurements. Using the ASI120MM mini camera as an example, a readout time per row of approximately 66 µs has been calculated. The error introduced, if the occultation is measured on row 1000 and the readout time per line is not taken into account, is 66 ms, which in some applications may be unacceptable.

If the camera used for the occultation is a rolling shutter camera, which is in fact the most common, knowing the impact of the rolling shutter described above, it is possible to improve the timestamp of our measurement by adding to the timestamp of the image the result of multiplying the readout time per row by the row number of the centroid where the occultation occurs.

But Table 3 shows that the correction due to the readout time is not the only one to take into account, except if small ROI's are used. The recommendation is to characterize our system in order to be able to apply the correction properly. To do this, we recommend a scenario similar to the one used in this study, in which we have verified that during the tests the PC was very well synchronised (average offset less than one millisecond) and with the stroboscopic method we can measure the offset of our configuration: camera, ROI, approximate line on which the concealment is going to be measured, binning, etc. This measurement, repeated to check that it is stable, reveals the offset to be applied to the timestamp we measure in the occultation. In addition, if possible, this measurement can be made before and after the occultation to include an eventual offset of the PC. It only takes 5 minutes to make a measurement with this method.

It should be noted that these rolling shutter considerations do not apply to cameras with global shutter as is the case for cameras with CCD sensors and CMOS with global shutter.

Summary

The described method, based on a stroboscopic effect, allows us to measure the deviation of the timestamp of our system with sub-millisecond precision respect to a PPS signal coming from a GPS, in a simple (by just placing a LED in front of the telescope) and cheap (the cost of the flash generator can be around 60 €) way. Any available device that generates a 500 ms pulse synchronised with PPS can be used.

The image processing procedure for the calculation of the deviations is also very simple as it only requires the photometry (for instance using *Tangra* or *PyMovie*/*PyOTE*) of the area of the image where we are going to do the occultation to generate a light curve. With a *Python* script it is easy to calculate the deviation.

This method allows us to analyse the offset time generated by our setup, i.e. the computer with its synchronisation mechanism, the software and the camera. On the other hand, it allows us to know if any corrections need to be made to our observations, by measuring the delay/ahead minutes before and after the event.

Finally, the importance of considering the effect of the rolling shutter in most CMOS cameras has been highlighted, especially in captures with ROIs of many rows. It has been explained how to calculate the readout time per row (two possible methods, both stroboscopic and with a lamp connected to AC power such as a Neon) and how to use this data to report a more accurate timestamp.

It should be noted that this method is only useful for measuring small deviations (less than 500 ms) and therefore it is necessary that the PC used for the measurements has an adequate synchronisation system.

References

[1] Rommel, F. L. et al. Stellar occultations enable milliarcsecond astrometry for trans-neptunian objects and centaurs. A&A, 644 A40 (2020) https://doi.org/10.1051/0004-6361/202039054

[2] https://www.qhyccd.com/qhy174gps-imx174-scientific-cooled-camera/

[3] Niu, X. et al., Quality evaluation of the pulse per second (pps) signals from commercial gnss receivers. GPS Solutions, 19:141–150, 01 (2014), https://doi.org/10.1007/s10291-014-0375-7

[4] Barry, M. A. et al., Verifying timestamps of occultation observation systems (2015), https://www.cambridge.org/core/journals/publications-of-the-astronomical-society-of-australia/article/verifying-timestamps-ofoccultation-observation-systems/F71907D2D928CE75150FA8E629D8A126

[5] Kamiński, K. et al., Reaching submillisecond accuracy in stellar occultations and artificial satellite tracking. Publications of the Astronomical Society of the Pacific, 135(1044):025001 (February 2023) https://iopscience.iop.org/article/10.1088/1538-3873/acacc8

[6] https://www.zwoastro.com/product/asi183/

[7] https://www.zwoastro.com/product/mini-cameras/

[8] https://learn.adafruit.com/adafruit-ultimate-gps-logger-shield/overview

[9] https://store.arduino.cc/collections/boards-modules/products/arduino-uno-rev3-smd?pos =7f id = e49402708ss = c

[10] https://static.garmin.com/pumac/GPS_18x_Tech_Specs.pdf

[11] https://www.thorlabs.com/thorProduct.cfm?partNumber=PDA10A

[12] https://www.keysight.com/us/en/product/DSOX3024T/oscilloscope-200-mhz-4-analog-channels.html

[13] Meinberg NTP software, https://www.meinbergglobal.com/english/sw/

[14] Stirk, A., 5 minute guide to making a GPS Locked Stratum 1 NTP Server with a Raspberry Pi, https://ava.upuaut.net/

[15] Glover, R. SharpCap software, https://www.sharpcap.co.uk/

[16] Pavlov, H. Tangra software, http://www.hristopavlov.net/Tangra3/

[17] Anderson, B., PyMovie software https://occultations.org/observing/software/pymovie/

[18] Gurgul, A. et al., LightStream – enhancements to the Astrometry24.NET software for processing SST and asteroid images from CCD and CMOS. In 2nd NEO and Debris Detection Conference, page 76 (January 2023)

Annexes

```
// ************************************************************************************************
// Arduino program to generate a 500ms pulse synchronized with the PPS signal from a GPS
// ************************************************************************************************
const byte PPS = 2;
const byte LED = 3;

int PPSflag=0;

void setup() {

 pinMode(PPS, INPUT);
 pinMode(LED, OUTPUT);

 // At start-up, the LED lights up for 2s.
 digitalWrite(LED, HIGH);
 delay(2000);
 digitalWrite(LED, LOW);

 // Activation of the interrupt on detection of the rising edge of the PPS signal
 attachInterrupt(digitalPinToInterrupt(PPS), PPSInt, RISING);
}

void loop() {
 if (PPSflag){
    PORTD |= B00001000;
    delay(500);
    PORTD &= B11110111;
    PPSflag=0;
 }
}

// interrupt routine
void PPSInt(){
 PPSflag=1; // to 1 if a rising edge has been detected
}
```

```
# ********************************************************************************************************************************************
# Python script to parse the csv file generated by Tangra and calculate the following timestamp by the stroboscopic method.
#  This script allows to automatically analyses the light curve of the stroboscopic capture
# The ".. name of the file.csv" must be replaced by the name of the csv file exported with Tangra.
# The variable PLOT_LINES allows to activate (set to True) or deactivate (set to False) the graphical representation
# The max_offset and min_offset variables allow to set the maximum and minimum points used for the regression lines.
# The script prints the results of all maxima and minima, as well as the mean, variance and standard error of the measurements.
# ********************************************************************************************************************************************

import os
import pandas as pd
import numpy as np
import matplotlib.pyplot as plt
from scipy.stats import linregress
from scipy.signal import find_peaks
import matplotlib.dates as mdates

res = []

# Function to find and analyze peaks in the data
def find_minmax(df, sign, texto):

  # Find peaks based on the sign
  if sign == 1:
     peaks, _ = find_peaks(df["Value"], width=10)
  else:
     peaks, _ = find_peaks(-df["Value"], width=10)

  for indice in peaks:

     # Print the value, time, and frame of the peak
     print(f'Value: {df.iloc[indice]["Value"]}, Time: {df.iloc[indice]["Time"]}, Frame: {df.iloc[indice]["Frame"]}', texto)

     # Define maximum and minimum offset for line fitting
     max_offset = 15
     min_offset = 10

     # Fit the line before the peak
     offset = max_offset
     while True:
        recta1 = df.iloc[indice - offset:indice - 1]
        if recta1.shape[0] == (offset - 1):
           break
        else:
           offset = offset - 1
           if offset < min_offset:
              return

     # Fit the line after the peak
     offset = max_offset
     while True:
        recta2 = df.iloc[indice + 1:indice + offset]
        if recta2.shape[0] == (offset - 1):
           break
```

```
    # Fit the line after the peak
        offset = max_offset
        while True:
            recta2 = df.iloc[indice + 1:indice + offset]
            if recta2.shape[0] == (offset - 1):
                break
            else:
                offset = offset - 1
                if offset < min_offset:
                    return

        # Calculate the regression lines before and after the peak
        x1_values = (recta1["Time"].dt.microsecond / 1e6).values
        y1_values = recta1["Value"].values
        slope1, intercept1, _, _, _ = linregress(x1_values, y1_values)

        x2_values = (recta2["Time"].dt.microsecond / 1e6).values
        y2_values = recta2["Value"].values
        slope2, intercept2, _, _, _ = linregress(x2_values, y2_values)

        # Find the intersection point of the two regression lines
        x_intersection = (intercept2 - intercept1) / (slope1 - slope2)
        y_intersection = slope1 * x_intersection + intercept1
        res.append(x_intersection)

        # Plot the results if PLOT_LINES is True
        PLOT_LINES = True
        if PLOT_LINES:
            plt.plot(x1_values, y1_values, 'o-', linewidth=0.1, markersize=4)
            plt.plot(x2_values, y2_values, 'o-', linewidth=0.1, markersize=4)

            specific_point_x = df.iloc[indice]["Time"].microsecond / 1e6
            specific_point_y = df.iloc[indice]["Value"]
            plt.scatter(specific_point_x, specific_point_y, color='black', s=20)

            plt.plot([x1_values[0], x_intersection], [y1_values[0], y_intersection], 'r--', label='Left regression line')
            plt.plot([x_intersection, x2_values[-1]], [y_intersection, y2_values[-1]], 'g--', label='Right regression line')

            plt.xlabel("Time(s)")
            plt.ylabel("ADU")
            plt.legend()

            plt.show()

# Load the CSV file
df = pd.read_csv(".. name of the file.csv", skiprows=14)

# Rename the columns
df.columns = ["Frame", "Time", "Value", "Background"]

# Clean and format the Time column
df["Time"] = df["Time"].str.strip("[]")
df["Time"] = pd.to_datetime(df["Time"], format="%H:%M:%S.%f")
```

```
# Separate even and odd rows
df_pares = df[df.index % 2 == 0].reset_index(drop=True)
df_impares = df[df.index % 2 != 0].reset_index(drop=True)

# Find peaks and calculate intersection for even rows
find_minmax(df_pares, 1, "even")
find_minmax(df_pares, -1, "even")

# Find peaks and calculate intersection for odd rows
find_minmax(df_impares, 1, "odd")
find_minmax(df_impares, -1, "odd")

# Process the results to calculate the final values
for i in range(len(res)):
    Value = res[i]
    off1 = Value - 0.250
    off2 = Value - 0.750
    if abs(off1) < abs(off2):
        res[i] = 1000 * off1
    else:
        res[i] = 1000 * off2

# Calculate the mean
mean_value = np.mean(res)
# Calculate the standard deviation
std_dev = np.std(res)
# Calculate the standard error
std_error = np.std(res) / np.sqrt(len(res))

# Print the results
for Value in res:
    print("{:.4f}".format(Value), " ms")

print("N:", len(res), "Avg", round(mean_value, 4), "std:", round(1000 * std_dev, 0), "microsec", "error:", round(1000 *
std_error, 0), "microsec")

# Plot the even and odd values
plt.figure(figsize=(10, 5))

plt.plot(df_pares["Time"], df_pares["Value"], 'o-', label='Even values', linewidth=0.1, markersize=1, color='red')
plt.plot(df_impares["Time"], df_impares["Value"], 'o-', label='Odd values', linewidth=0.1, markersize=1,
color='blue')

# Format the x-axis and y-axis
plt.gca().xaxis.set_major_formatter(mdates.DateFormatter('%H:%M'))
plt.ticklabel_format(style='plain', axis='y')
plt.legend()

plt.xlabel('Time(s)')
plt.ylabel('Value (ADU)')
plt.grid(True)
plt.show()
```

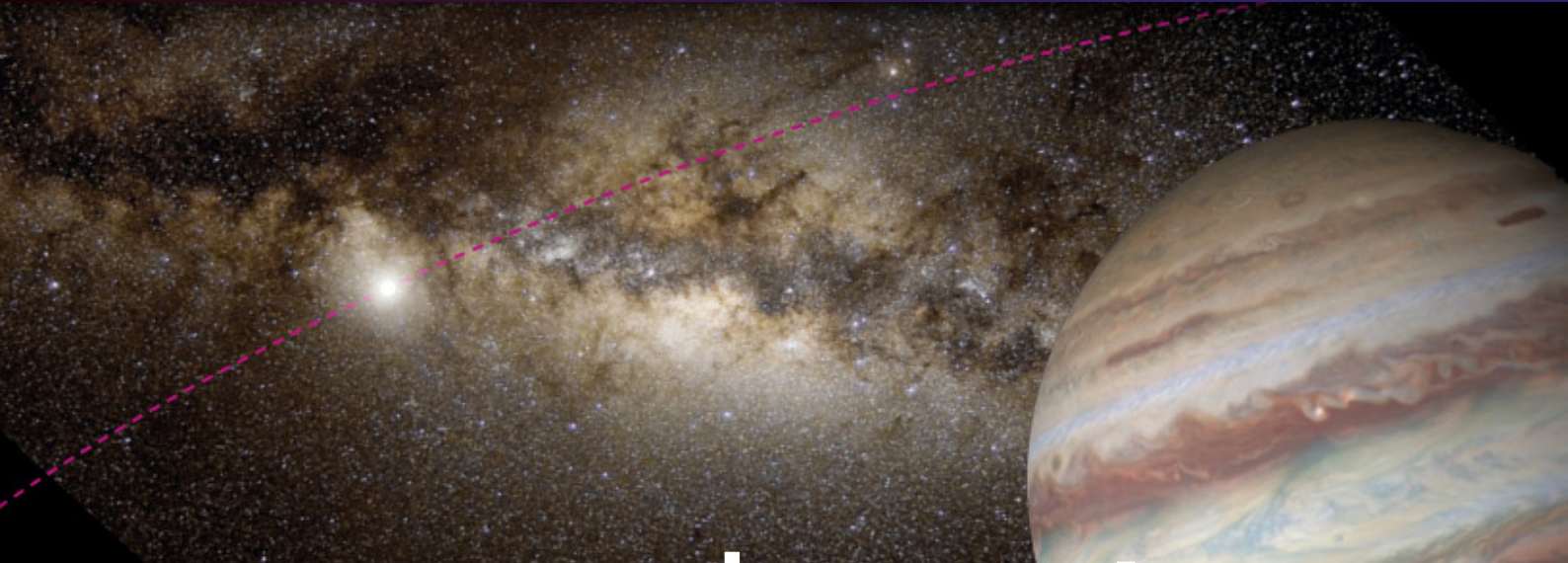

Beyond Jupiter

The World of Distant Minor Planets

Since the downgrading of Pluto in 2006 by the IAU, the planet Neptune marks the end of the zone of planets. Beyond Neptune, the world of icy large and small bodies, with and without an atmosphere (called Trans-Neptunian Objects or TNOs) starts. This zone between Jupiter and Neptune is also host to mysterious objects, namely the Centaurs and the Neptune Trojans. All of these groups are summarised as "distant minor planets". Occultation observers investigate these members of our solar system, without ever using a spacecraft. The sheer number of these minor planets is huge. As of 2024 September 30, the *Minor Planet Center* listed 1727 Centaurs and 3546 TNOs.

In the coming years, JOA wants to portray a member of this world in every issue; needless to say not all of them will get an article here. The table shows you where to find the objects presented in former JOA issues. (KG)

In this Issue:

(541132) Leleākūhonua

Konrad Guhl · IOTA/ES · Berlin · Germany · kguhl@astw.de

ABSTRACT: Since 2016, JOA regularly publishes portraits of objects beyond Jupiter's orbit. This short communication on the extreme trans-Neptunian object (ETNO) (541132) Leleākūhonua tells the story of its discovery, the meaning behind its name and its orbit. Size and physical properties are taken from the latest published data, although it was last observed astrometrically in 2018.

No.	Name	Author	Link to Issue
944	Hidalgo	Oliver Klös	JOA 1 2019
2060	Chiron	Mike Kretlow	JOA 2 2020
5145	Pholus	Konrad Guhl	JOA 2 2016
5335	Damocles	Oliver Klös	JOA 2 2023
7066	Nessus	Konrad Guhl	JOA 1 2024
8405	Asbolus	Oliver Klös	JOA 3 2016
10370	Hylonome	Konrad Guhl	JOA 3 2021
10199	Chariklo	Mike Kretlow	JOA 1 2017
15760	Albion	Nikolai Wünsche	JOA 4 2019
15810	Awran	Konrad Guhl	JOA 4 2021
20000	Varuna	Andre Knöfel	JOA 2 2017
28728	Ixion	Nikolai Wünsche	JOA 2 2018
32532	Thereus	Konrad Guhl	JOA 1 2023
38628	Huya	Christian Weber	JOA 2 2021
47171	Lempo	Oliver Klös	JOA 4 2020
50000	Quaoar	Mike Kretlow	JOA 1 2020
53311	Deucalion	Konrad Guhl	JOA 2 2024

No.	Name	Author	Link to Issue
54598	Bienor	Konrad Guhl	JOA 3 2018
55576	Amycus	Konrad Guhl	JOA 1 2021
58534	Logos & Zoe	Konrad Guhl	JOA 4 2023
60558	Echeclus	Oliver Klös	JOA 4 2017
90377	Sedna	Mike Kretlow	JOA 3 2020
90482	Orcus	Konrad Guhl	JOA 3 2017
120347	Salacia	Andrea Guhl	JOA 4 2016
134340	Pluto	Andre Knöfel	JOA 2 2019
136108	Haumea	Mike Kretlow	JOA 3 2019
136199	Eris	Andre Knöfel	JOA 1 2018
136472	Makemake	Christoph Bittner	JOA 4 2018
174567	Varda	Christian Weber	JOA 2 2022
208996	2003 AZ_{84}	Sven Andersson	JOA 3 2022
341520	Mors-Somnus	Konrad Guhl	JOA 4 2022
471143	Dziewanna	Wojciech Burzyński	JOA 3 2024
486958	Arrokoth	Julia Perła	JOA 3 2023
-	2004 XR_{190}	Carles Schnabel	JOA 1 2022

The Discovery

The object, also known as a 'sednoid' was discovered on 2015 October 13 in a survey for objects beyond the Edgeworth-Kuiper Belt cliff. This survey uses the 8.2-m *Subaru Telescope* (Mauna Kea, Hawaii) in the northern hemisphere with the 1.5-degree field of view provided by its Hyper Suprime-Cam (HSC). The survey is also conducted in the southern hemisphere with the 4.0-m Victor M. Blanco telescope (at *Cerro Tololo Inter-American Observatory* (CTIO)) employing its Dark Energy Camera (DECam) having an even bigger 2.7 square degree field. The discovery was made by D. Tholen, C. A. Trujillo, and S. S. Sheppard and assigned the preliminary designation, 2015 TG_{387}.

At this time the objet was about 80 AU distant (double the semi-major axis of Pluto) and had a brightness of magnitude 24.0 in the r-band. Later, the object was identified from its orbit as an extreme trans-Neptunian object (ETNO).

Figure 1. The Hyper Suprime-Cam (HSC) and the primary mirror of the 8.2 m Subaru Telescope. The image of a larger lens of HSC's Wide Field Corrector (WFC) is seen on the primary focus. (Credit: Kazuhito Dobashi/NAOJ)

The Name

The object was numbered 541132 by the MPC on 2019 October 10 [1]. Because of the provisional designation TG, it was given the nickname "the goblin" before its final designation. On 2020 June 3, it received its official name [2] suggested by linguists and referring to the life form mentioned in the Hawaiian creation chant, called 'the Kumulipo'. The name refers to a bird, the kolea, or Pacific golden plover, which on migrating travels large distances, and also evokes a yearning to be near Earth. This is by way of analogy to the extreme orbit of (541132) Leleākūhonua.

The Orbit

The orbit is extremely eccentric (0.952) and inclined to the ecliptic by 11.7° (Figure 2). With a semi-major axis of ~1300 au, the distance from the Sun is between 65 au and ~2600 au. Currently, Leleākūhonua is 76 au from the Sun (approximately 2.5 times the distance of Neptune) on the way towards perihelion. The body reaches perihelion during early 2078. The orbital period is so great that the date of its following perihelion is rather uncertain being some 40,000 to 55,000 years into the future! Theories explain the orbit by a close encounter of the early solar system with a passing star.

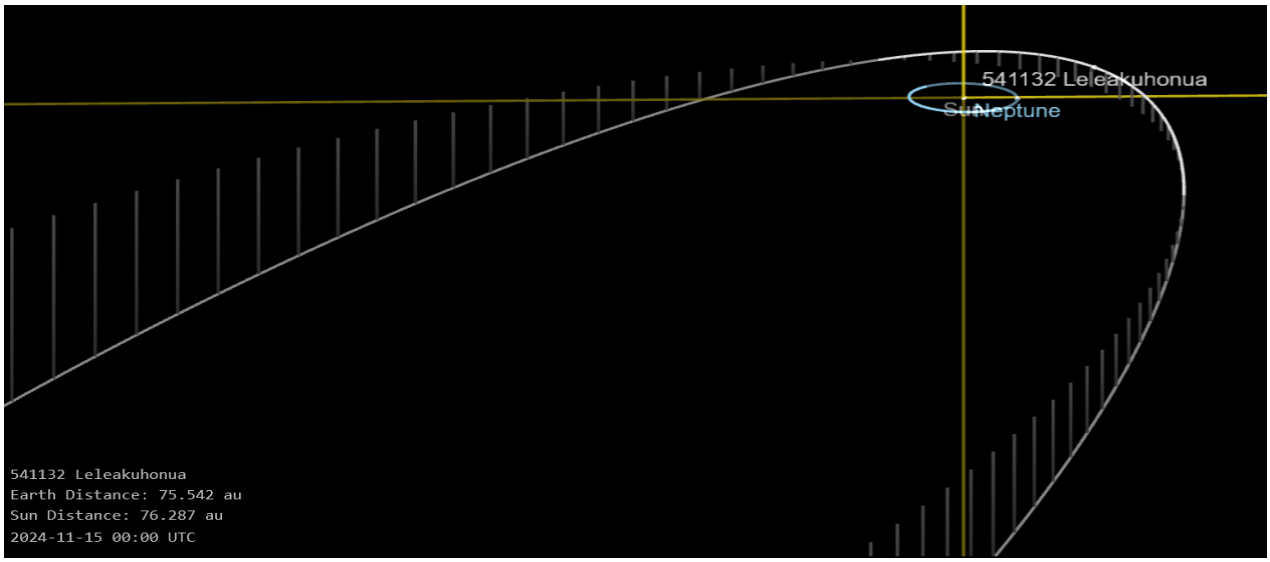

Figure 2. Orbit diagram and position of (541132) Leleākūhonua on 2024 November 15.
(Source: NASA/JPL Small-body database lookup, https://ssd.jpl.nasa.gov/tools/sbdb_lookup.html#/?sstr=541132

After the discovery of Sedna and 2012 VP_{113}, the object (541132) Leleākūhonua was the third discovered member of the inner Oort cloud, which is defined as a family of TNOs with perihelion distances of q ≳ 50 au and semimajor axes of a ≈ 150 – 3000 au. With a value of q > 50 au, (541132) Leleākūhonua is a member of the "Sednoids" group.

The value of q > 50 may seem to have been chosen arbitrarily. This is not the case, because the objects in the 2:1 resonance with Neptune (q ~ 48 au) are excluded from this classification.

The longitude of perihelion for (541132) Leleākūhonua is between the perihelion of (90377) Sedna and that of 2012 VP113 (still unnumbered) and thus similar to the main group of clustered extreme trans-Neptunian objects (ETNOs). It has been suggested that this could be an indication of a massive, distant undiscovered object often referred to as 'Planet X' [3].

Physical Characteristics

The first estimation of its diameter was calculated from its brightness and distance at 80 au, assuming a moderate albedo of 15%, giving a value of 300 km. The absolute magnitude [H] is reported to be 5.57 [4].

At this point, there have been no moons discovered orbiting this ETNO. A rotation light curve has also not yet been published.

Occultations by (541132) Lelākūhonuae

In 2018, a stellar occultation by (541132) Leleākūhonua was successfully observed in co-operation with the teams of Lucky Star and RECON [5].

The occulted star (Gaia DR3 source ID 2767694522024100608) has a G magnitude of 14.45. Of the 14 stations, 10 provided data but only one station was successful. A single occultation chord lasting 7.8 s and a nearby nondetection yielded constraints for its size and albedo thereby providing two solutions. The derived radius is between 100 and 124 km (circular profile) and suggests an albedo in the range of 0.16–0.24.

Future

Given that the last astrometric observation of this body was in 2018, it is not possible to accurately predict future stellar occultations. Clearly, it is time that it was recovered so that its current rather uncertain orbit can be improved to an accuracy sufficient for us to identify and observe potential occultations into the future. Its next opposition is on 2025 March 31 in Pisces and remains close to magnitude 24.5V all year. The innovative 8.4-m aperture wide-field 'Simonyi Survey Telescope' housed in the *Vera C. Rubin Observatory* (formerly known as the *Large Synoptic Survey Telescope* or LSST) is nearing completion in Chile, and is scheduled to start full survey operations during late 2025 [6].

It is hoped it will recover this object and find many more sednoids additional to the current three that have already been found. It is expected to increase the number of catalogued objects by a factor of 10–100, enabling many more stellar occultations of distant objects to be successfully observed as well as help with the search for the hypothesized Planet X.

References

[1] Minor Planet Circ. 117077
https://www.minorplanetcenter.net/iau/ECS/MPCArchive/2019/MPC_20191010.pdf
[2] Minor Planet Circ. 123453
https://www.minorplanetcenter.net/iau/ECS/MPCArchive/2020/MPC_20200603.pdf
[3] Sheppard, S. et. al.: A New High Perihelion Inner Oort Cloud Object: 2015 TG387, Astronomical Journal 135, p55–67.
https://arxiv.org/abs/1810.00013
[4] Minor Planet Circulars Orbit Supplement 701700
https://www.minorplanetcenter.net/iau/ECS/MPCArchive/2022/MPO_20220520.pdf
[5] Buie, M. et al.: A Single-chord Stellar Occultation by the Extreme Trans-Neptunian Object (541132) Leleākūhonua, The Astronomical Journal vol 159, Number 5
https://iopscience.iop.org/article/10.3847/1538-3881/ab8630
[6] https://en.wikipedia.org/wiki/Vera_C._Rubin_Observatory

Useful Links

About objects like TNOs and Centaurs:

NASA/JPL Small-Body Database Lookup
http://ssd.jpl.nasa.gov/sbdb.cgi
Spacewatch, Lunar and Planetary Laboratory, University of Arizona
http://spacewatch.lpl.arizona.edu
Minor Planet Center
http://www.minorplanetcenter.org

Observation Campaign for Mutual Events of the Saturnian Satellites

Arnaud Leroy, Uranoscope de l'Ile de France, has provided on 2024 September 9th via Planoccult a link to predictions of mutual events of the satellites of Saturn:

http://www.astrosurf.com/whitebridge/phesat/index_phesat.html

On this website you can find predictions for the best events for France and nearby countries.

Predictions for other locations can be calculated here:

IMCCE-SAI: Natural Satellites Services. Ephemerides of the mutual eclipses and occultations of the main satellites of Saturn in 2024-2026
http://nsdb.imcce.fr/multisat/nsszph6he.htm

The campaign for those events is a part of a pro-am collaboration with Paris Observatory.

Contacts:

Paris Observatory:
Vincent Robert - vincent.robert@obspm.fr

Amateur part:
Michael Irzik - michael.irzyk@laposte.net,
Arnaud Leroy - arnaudastro@yahoo.fr

Vincent Robert, Paris Observatory, will collect the data. Please inform him via e-mail if you have observed an event and you want to share data.

(O.Klös)

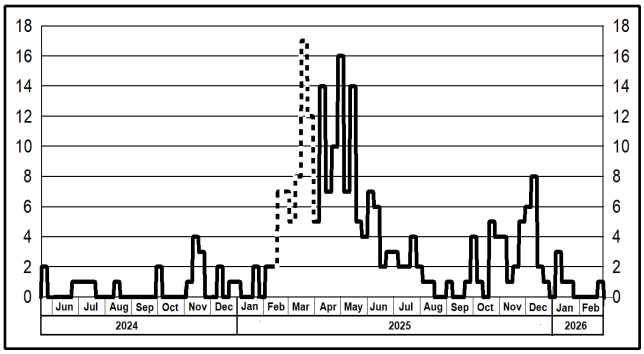

Figure 1. The number of events per week (Monday to Sunday). Only 30% of the events can be seen from any single observatory. Events between 2025 February 15 and 2025 March 31 are not observable (twilight). (Credit: Jean-Eudes Arlot (IMCCE), Nicolai Emelyanov (SAI))

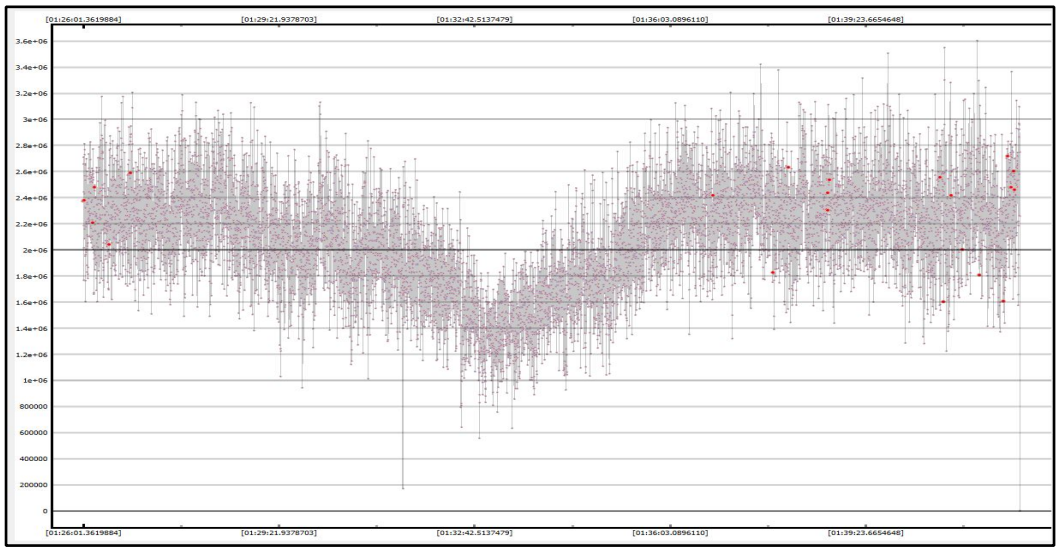

Figure 2. Tethys occulted by Enceladus on 2024 June 24 with an almost perfect annular occultation (impact = 0.004), lasting 5.64 min. Saturn was 18° above the horizon. The observation was carried out near Lille, France, using a 406 mm-diameter, 1,800 mm focal length Dobsonian telescope equipped with a Televue Powermate X2 lens and an unfiltered QHY174M-GPS camera, exposure time 0.1 s. Lightcurve after reduction and normalisation with PyOTE. (Credit: Serge Vasseur, IOTA/ES)

News

New Lunar Occultation Coordinator for Europe

Dietmar Büttner has taken over the task of collecting and reducing total lunar occultations for Europe from Jan Mánek.

Büttner is an active observer of lunar occultations since 1978 and developed the algorithms for deriving the lunar limb profiles from the altitude measurements of the *Kaguya* and *Lunar Reconnaissance Orbiter* missions for provision and use in the *GRAZPREP* software by Eberhard Riedel. He also reported in the *Occultation Newsletter* and the *Journal for Occultation Astronomy* on the still valuable measurements of occultation phenomena on the limb of the Moon.

Some of Büttner's publications:

- Lunar limb profile models in the past and today
  Journal for Occultation Astronomy Vol. 5, No. 2, 2015-02,
  https://www.iota-es.de/JOA/joa2015_2.pdf
- A Renaissance of Lunar Occultations
  Journal for Occultation Astronomy Vol. 7, No. 2, 2017-02,
  https://www.iota-es.de/JOA/joa2017_2.pdf

Observers do not need to make any changes in their setup of *Occult*. The e-mail address LunOccult@IOTA-ES.de for reporting lunar occultation observations in Europe will continue to be valid.

The JOA editorial team would like to thank Jan Mánek for his many years of service for collecting and reducing the lunar occultation observations for Europe and wish Dietmar Büttner a good start in his new role. In addition to asteroidal occultations, all observers should also pay more attention to lunar occultations in the coming years.

(O.Klös)

First Version of the DVTI ADV Player is Available

Andreas Schweizer (SOTAS, IOTA/ES) provides a first version of the *ADV Player* as download on the DVTI+Cam webpage:

https://dvticam.com/support

He wrote on August 31st on Planoccult that the functionality of the first version of the application is limited, and it only runs on *Windows*. ADV files can be opened, viewed and exported in various file formats including mp4. Additionally, the metadata of the files will be displayed in this new software (Figure 1).

In the upcoming months, more features will be added.

Such as:

- Scaling the image
- Placing markers such as an arrow or circle on the image
- Histogram instead of background/range
- Opening and exporting other file formats such as SER and FITS sequence
- Support for *Linux*

Questions, bug reports and suggestions can be placed on the DVTI forum:

https://groups.io/g/d-vti-cam/messages

(O. Klös)

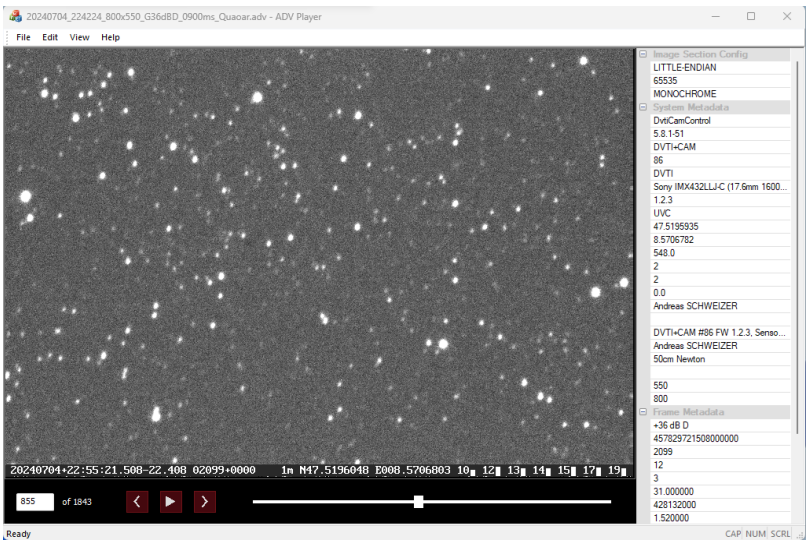

Figure 1. Screenshot ADV Player (DVTI forum)

Figure 1. Group photo in front of Stuttgart Planetarium (J. Löwe)

ESOP XLIII - Report of the 43rd European Symposium on Occultation Projects

Alex Pratt · IOTA/ES · BAA · Leeds · England · alex.pratt@bcs.org.uk
Oliver Klös · IOTA/ES · Eppstein-Bremthal · Germany · pr@iota-es.de

ABSTRACT: The 43rd European Symposium on Occultation Projects (ESOP) took place at Carl-Zeiss-Planetarium Stuttgart, Germany, during the weekend of August 24th – 25th and it was a hybrid event held simultaneously as an in-person meeting and an online video conference. A total of 60 delegates attended the meeting, some accompanied by family members, and 21 persons participated online, altogether representing Algeria, Australia, Belgium, Czechia, France, Germany, Greece, Ireland, Italy, Poland, Spain, Türkiye, the United Kingdom and the USA. The science meeting was followed by social excursions on the Monday and Tuesday.

Friday 23rd August 2024

Registration and the welcome reception took place at Sternwarte Stuttgart, one of the oldest public observatories in Germany, sited on the Uhlandshöhe, a hill to the east of the city. Registration opened from 5 pm to 6:30 pm where each delegate collected their conference badge and a folder containing travel information, the symposium programme, a notepad and pen, booklets on the planetarium and observatory and a ticket for the TV tower, and it was a first opportunity for them and accompanying persons to meet old friends and make new ones.We were treated to a buffet meal, including Swabian ravioli and potato salad, and we had plenty of time to view the observatory's facilities and range of telescopes. Andreas Eberle, chairman of the Swabian Observatory Association and lead member of the Local Organising Committee, welcomed everyone to the reception and outlined the upcoming programme of events.

Figure 2. A sunny welcome reception at Stuttgart Observatory. (O. Klös)

Figure 3. Andreas Eberle welcomes the participants. (O. Klös)

Saturday 24th August 2024

The registration desk opened again at 8:30 am for delegates to collect their name badges and folders, then proceed into the Keplersaal where the conference would take place.

At the opening ceremony we were welcomed by Uwe Lemmer, Director of Carl-Zeiss-Planetarium Stuttgart, by Andreas Eberle who also greeted the online attendees, and also by Konrad Guhl, President of IOTA/ES.

Remembrance - Eberhard Bredner requested that everyone joined him in the traditional IOTA-ES manner to pay tribute to our late friend and colleague, Jan-Maarten Winkel (1961-2024).

The accompanying persons not taking part in the symposium now joined their separate programme led by Klaus Mayer and Dorothee Schaefer.

Session 1 - chaired by Konrad Guhl

When the Stars make Surprises – Anna Marciniak, Christian Weber (presented by Anna Marciniak)

Stellar occultations by minor bodies can cause unexpected effects. Anna discussed various light curve examples, including double dips indicating the discovery of a double star and submitting a paper to JDSO. If only one component of a double star is occulted it can give a smaller drop than expected. Caution is required because a grazing event can produce diffraction effects not caused by a binary star. These can be processed in *AOTA* and *PyOTE*.

(During the Q&A sessions a 'softball' cube – containing a microphone - was thrown towards the questioner. This was a source of amusement during the symposium because not everyone had a good aim and some delegates weren't looking, so they were hit by the cube!)

The occultation of UCAC4 440-126076 (11m.4) by Neptune and its rings on the 9th of October 2024 (presented by Wolfgang Beisker)

In the early hours of 2024 October 9th (European time), Neptune will occult a mag. 11.4 star, visible from a large part of the Earth. Wolfgang explained that it will be a difficult observation because Neptune is about 3.5 magnitudes brighter than the star. He showed the spectral response of Neptune, it is dark in the methane band, so he recommends using a NIR filter, i.e. for wavelengths longer than 850nm, such as a CH4 filter. However, many cameras have low sensitivity in this region, so he suggests using one with an IMX462C CMOS chip. This combination should optimise the light drop to 1 mag.

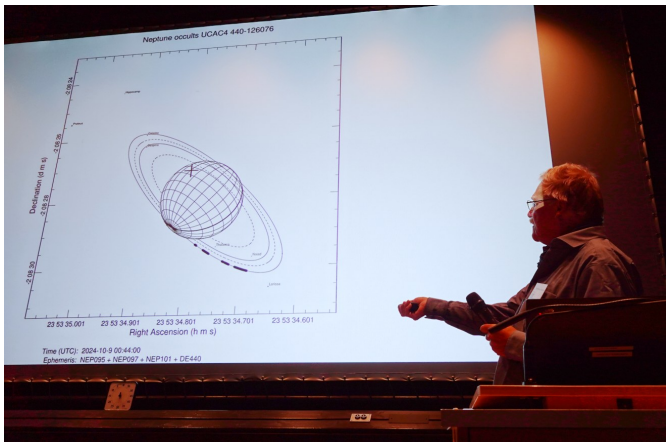

Figure 4. The occultation by Neptune and its rings presented by Wolfgang Beisker. (O. Klös)

An Occultation Event by Pluto at the IAS Observatory Hakos/ Namibia (presented by Karl-Ludwig Bath)

As Pluto moves slowly away from the Sun its atmosphere is thinning and freezing out. It is important to keep monitoring Pluto whenever an occultation opportunity arises, because light curves of the gradual disappearance and reappearance of a star occulted by Pluto give valuable data for studies of Pluto's atmosphere. Karl-Ludwig described a successful observation made on 2024 August 4th from the IAS Observatory in Namibia.

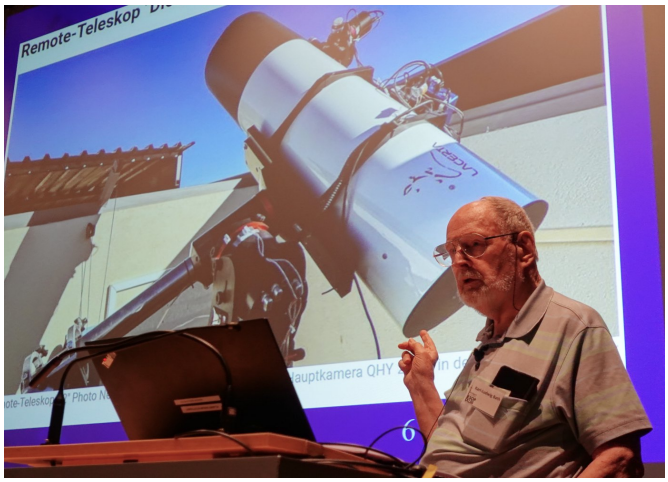

Figure 5. Karl-Ludwig Bath shows an image of the remote telescope used for the observation. (O. Klös)

Recent Czech observations (presented by Jiří Kubánek)

Czech observers are very active in occultation studies and Jiří described their most notable achievements in the past twelve months: two asteroidal satellite discoveries, (5457) Queen's and (100624) 1997 TR28; one double star detection (UCAC4 560-045206); observation of the annular occultation of Betelgeuse, a grazing occultation by (16583) Oersted, an occultation by the NEA (1036) Ganymed) and two other interesting cases by asteroids (6075) Zajtsev and (210) Isabella, where secondary events can be irregularities in the asteroid.

Pleading: Do not forget about Lunar Occultations – New Aspects – New Tools (presented by Eberhard Riedel)

Eberhard made a plea for observers to continue recording lunar occultations. There is still valuable work to be done – uncertainties and errors remain in the lunar topography, there are gaps in the LRO/LOLA data, and the precision level used in reductions is also a factor. He demonstrated his latest release of GRAZPREP, urged observers to use it and to send their occultation timings to the new European coordinator, Dietmar Büttner (see News in this issue of JOA).

Session 2 - chaired by Stefan Benz

Observation of the Betelgeuse occultation in Spain (presented by Carles Schnabel)

As an introduction, Carles described the successful observation of the occultation by (319) Leona on 2023 September 13th which greatly helped in the preparations for its encounter with Betelgeuse on December 12th, three months later. He presented the work of Spanish observers in recording the Betelgeuse-Leona event, including their light curves and the large set of chords from SODIS and *Occult*, with particular mention of the northernmost chord obtained by our late friend Jan-Maarten Winkel. Carles said he

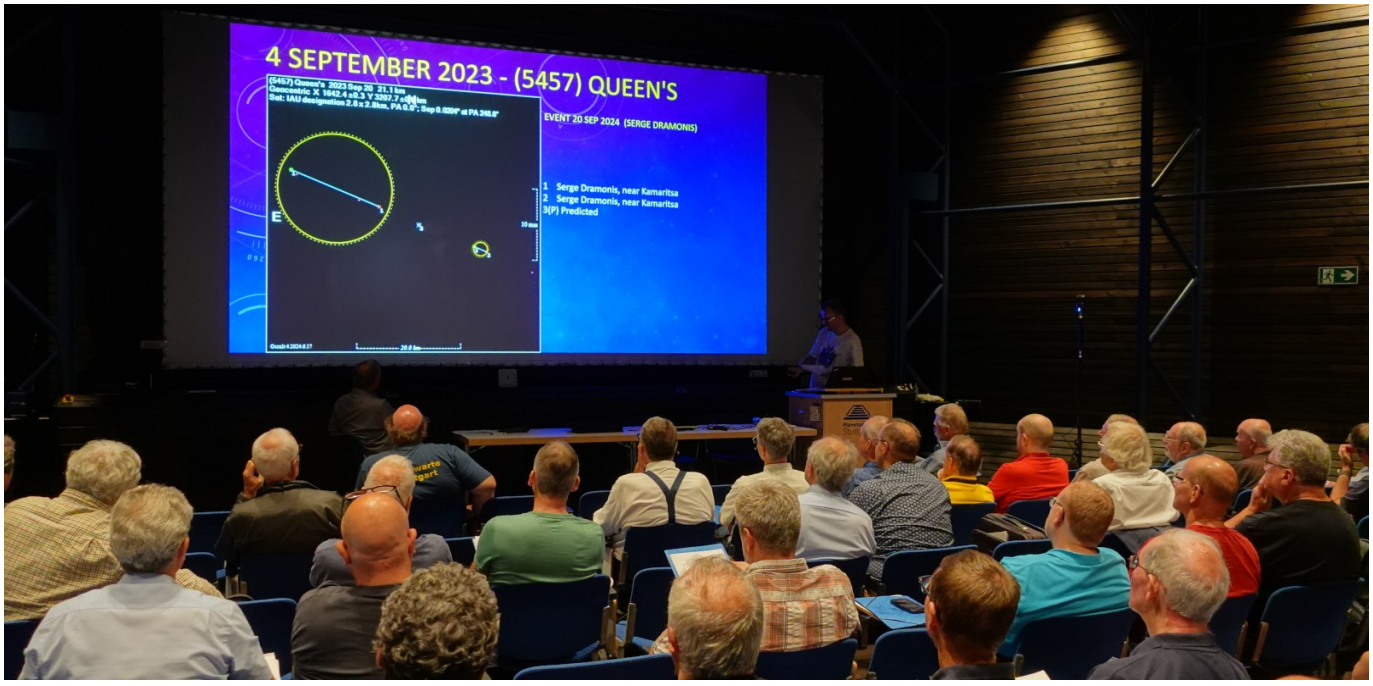

Figure 6. In the Kepler Hall, Jiří Kubánek shows the chords of the detection of the satellite of asteroid (5457) Queen's. (O. Klös)

and his colleagues are assisting with the analysis of the observations by the Instituto de Astrofísica de Andalucía and the Observatoire du Paris. Over 100 light curves were received but many were affected by varying amounts of cloud cover.

The Algerian participation in Spain for the Observation of Betelgeuse Occultation by Asteroid (319) Leona on December 12th , 2023 - Djounai BABA AISSA, Ridha LASSOUED, Hicham Rayane, Mohamed Lamine ALLIK, Lazhari SACI and El-Hadi SEFAR REMALI (presented by Djounai BABA AISSA)

Djounai summarised the circumstances of this rare event and said that he and five amateur astronomers travelled to Alicante, Spain to observe this special form of annular eclipse. They used a 127 mm Maksutov telescope on a motorized altazimuth mount lent by colleagues of the *Sabadell Observatory*, Spain, a Watec 910 HX/RC camera with IOTA-VTI time inserter and five Canon DSLR cameras on tripods. Observers were spread over a 10-kilometre strip around Alicante. They obtained six positive light curves and recorded the dip, although the foggy sky affected the S/N ratios, particularly the less-sensitive DSLRs. Their observed durations of the event matched the predictions and they were very pleased to contribute to this major pro-am campaign.

Figure 7. Djounai Babba Aissa reports about the Algerian participation in the (319) Leona occultation observation. (O. Klös)

Observing the Betelgeuse-Leona occultation from Spain and Portugal – Tim and Anne Haymes (UK), Michael O'Connell (IE), Alex Pratt (UK) - (presented by Alex Pratt)

These four observers selected locations in Spain and Portugal to record this rare event (Michael and Alex – El Plantio, Alicante, Spain - Tim and Anne - Colos, Portugal). Alex said they couldn't do much testing because of the bad weather but they chose QHY174M-GPS and Watec 910 cameras, 135mm telephoto lenses, a 40mm apo refractor and R and V filters. High thin clouds affected the Alicante sky, much less so in Colos, but they got useful recordings. "It was wonderful to look up and see Betelgeuse wink at us!" Their data were submitted to SODIS and the Occultation Portal and they also were pleased to see that Jan-Maarten Winkel submitted a valuable northernmost chord.

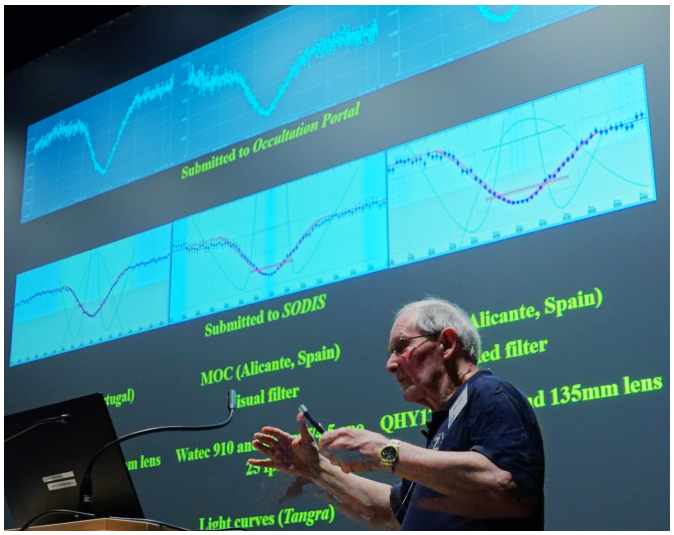

Figure 8. Alex Pratt presents lightcurves of the occultation of Betelgeuse by (319) Leona. (O. Klös)

Multi colour video observations of the Betelgeuse occultation on 12.12.23 (presented by Bernd Gährken and Peter Slansky)

Bernd and Peter said that they, along with three other German amateur observers, recorded the Betelgeuse event from three locations in southern Spain. As presented at last year's ESOP, they planned to use various equipment and filters to obtain multi-spectral recordings from which they could extract photometric/colourimetric curves in red, green, blue and near infrared. They explained the recording techniques they employed and presented and discussed their results.

Discussion: How to interest new observers to do occultation work (presented by Andreas Eberle)

Andreas said that hosting ESOP in Stuttgart was an ideal opportunity to use it to spark a local interest in occultations and to build an observing community. He discussed the experiences of the Sternwarte Stuttgart members and spoke about possible developments for the future.

This closed the sessions of the first day of ESOP XLIII.

Visit of the planetarium – the assembled group then moved into the adjacent planetarium for the showing of "Zeitreise – vom Urknall zum Menschen" (Time travel – from the Big Bang to humankind) The show was in German and audio guides in English were available. Everyone enjoyed this high-quality audio-visual experience which took us on a journey from the birth of the universe to the first stars and galaxies, the formation of our own Sun, its family of planets, our home planet Earth, the evolution of life, the age of the dinosaurs, through to modern-day humans, civilisation and technology.

We all gathered outside the planetarium for the traditional ESOP group photo (Figure 1), then travelled by tram to visit Stuttgart's Fernsehturm, its famous television tower. We used the lift in small groups to travel up to the observing platforms from where we could take in the wide vistas across the city and the surrounding area. The Stuttgart members pointed out the location of their observatory on the Uhlandshöhe and we were asked to wave because the observatory was using a telescope to take another group photo of us (Figure 9).

Figure 9. The most distant group photo ever taken at an ESOP. Sebastian Dittmann took the photo with a telescope at Stuttgart Observatory from a distance of 3 km.

Social dinner – we queued for the lift to go down to enjoy the Symposium dinner which was held in Leonhardt's restaurant at the foot of the Fernsehturm. This was another opportunity to chat with friends and discuss past, current and future projects.

Sunday 25th August 2024

The programme on Sunday started with the General Assembly of IOTA/ES. Members joined the General Assembly in person or online. After an introduction given by Konrad Guhl, scientific results and future projects were presented by Wolfgang Beisker. Secretary Nikolai Wünsche gave some member statistics. Oliver Klös talked about the latest statistics of the news feeds on Mas□ todon and X. During the Betelgeuse occultation, some members were very active with posting videos on online platforms. Andreas Tegtmeier presented the treasurer's report. Every two years, the Board of IOTA/ES has to be elected. The next election will take place in 2025.

Session 3 - chaired by Andreas Eberle

Results from Asteroid Shape Modelling Driven by Archival Stellar Occultation Data - Julia Perła, Adam Mickiewicz University in Poznań, Poland (presented by Julia Perła)

Julia described the subject of her Master's degree thesis which was to select asteroids which had good numbers of chords in the occultations dataset but were lacking in light curve data. Her project was to obtain light curves of selected asteroids with rich occultation data, apply the convex inversion technique, then scale the models against the occultation chords. The asteroids' diameters and dimensions could be determined, compared with results from IR studies and their shape models investigated.

Figure 10. Julia Perła compares diameters of asteroids from different sources. (O. Klös)

VAMOR to select and scale 3D models - Konrad Guhl, Frank Schaffer (presented by Frank Schaffer and Konrad Guhl)

Frank and Konrad expanded on their previous work presented in JOA 2022-03 and ESOP 2023. Their technique transposes occultation data into 3D-space, creating a virtual model of an asteroid, which can be scaled and rotated in 3-axes to find the best fit. They can model asteroids that are dimensionless or have a double-solution from light curve inversion. They showed results for (357) Hippo, (357) Ninina and (500 Selinor).

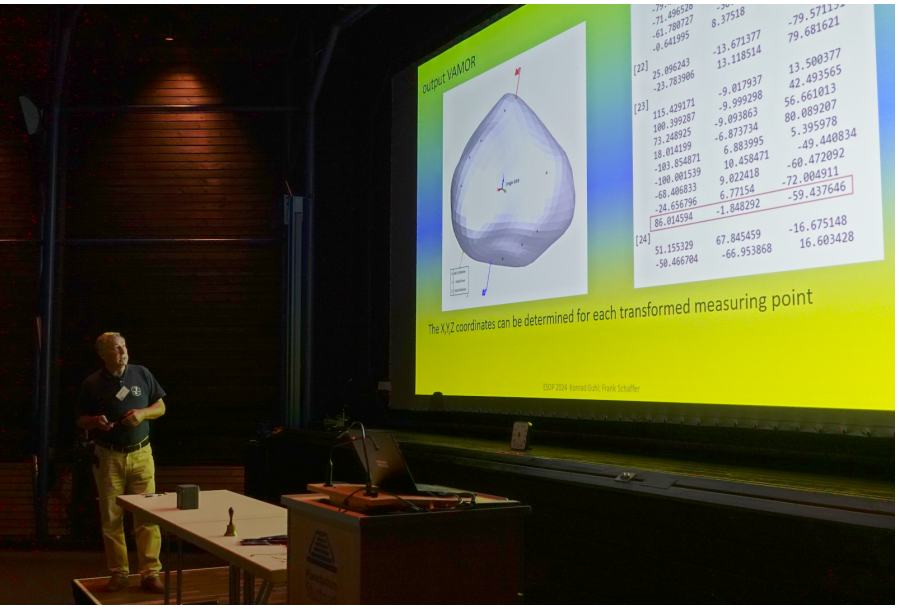

Figure 11. Konrad Guhl presents the status of the VAMOR project. (O. Klös)

Astronomical scintillation – causes, effects and possible mitigation (presented by Robert Purvinskis)

Robert explained how the Earth's atmosphere affects the signal from a light source on its journey to an observer, from the upper atmosphere down to ground level. He discussed the passage of a signal through these zones and he outlined modern measurement techniques which are under development to reduce the impact on photometry time series. Some may be useful for occultation observing in certain cases.

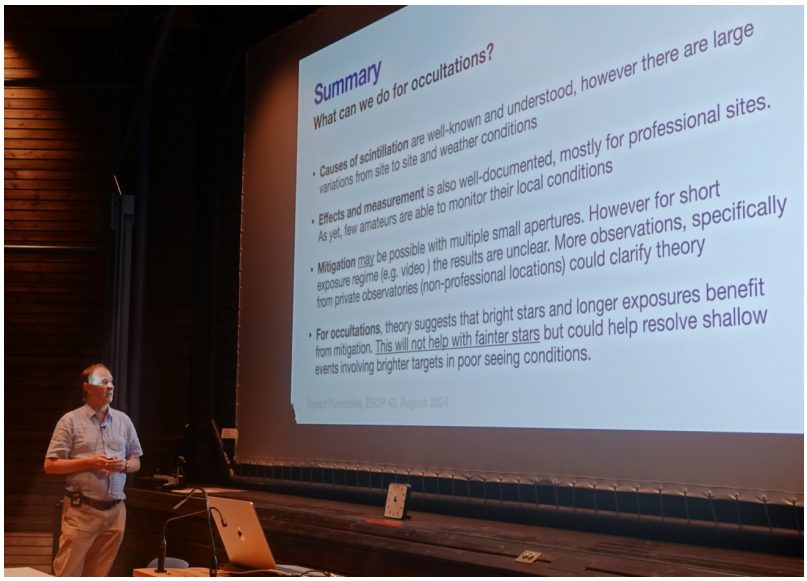

Figure 12. Robert Purvinskis summarises his presentation about astronomical scintillation effects during occultation observations. (O. Klös)

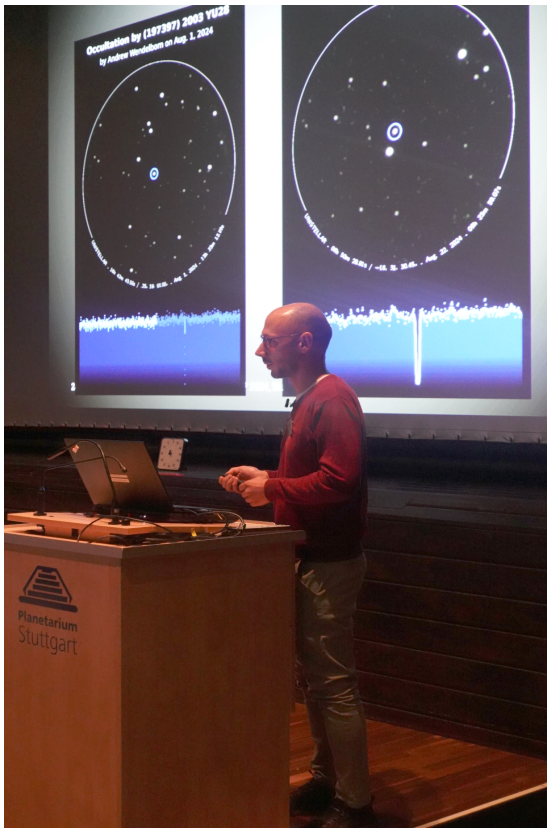

Figure 13. Josef Hanuš shows results of occultation observations by the Unistellar network. (O. Klös)

Session 4 - chaired by Wolfgang Beisker

Stellar occultations by the Unistellar network of citizen astronomers - Josef Hanuš, Franck Marchis, Ryan Lambert, Tom Esposito, Josef Ďurech (presented by Josef Hanuš)

Josef described the Unistellar network which is a worldwide community of about 10,000 citizen astronomers owning and operating eVscope and eQuinox telescopes. They are one of the new family of smart telescopes (up to 114mm aperture) with CMOS sensors designed for autonomous operation, minimising the need for manual intervention for setup and configuration. They are mainly used for deep sky, planetary and solar observing but Josef showed examples and results of asteroidal occultations recorded by the Unistellar network.

A short update about the Swiss DVTI+CAM project – (presented by Andreas Schweizer and Stefan Meister)

Andreas and Stefan demonstrated new features added to their camera control software and summarised ongoing developments in the functionality. They showed examples of events recorded with DVTI cameras and explained how their future-proof design allows the replacement of the sensor if the owner wishes to upgrade the camera. They discussed the models currently supported during the feedback and Q&A part of their presentation.

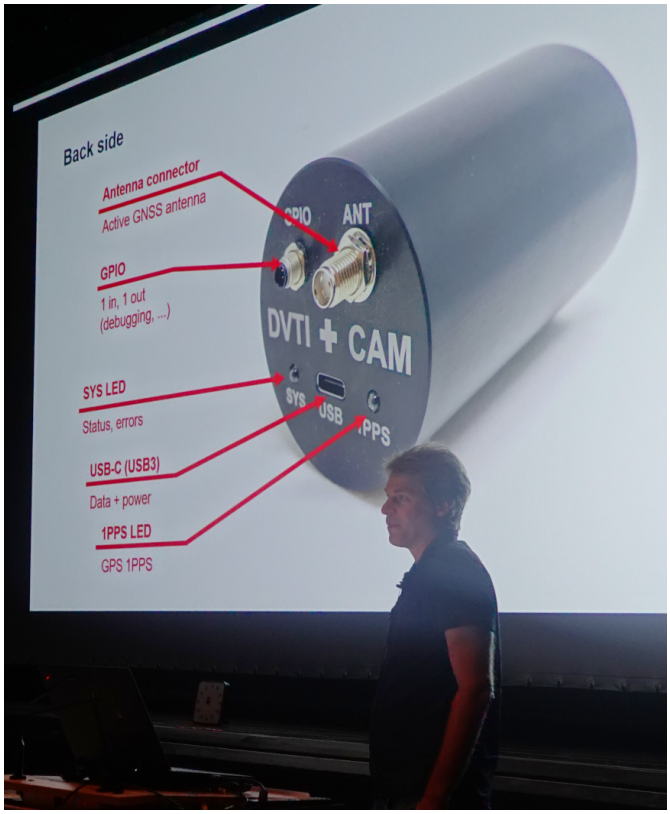

Figure 14. The latest technical developments of the DVTI+CAM are presented by Andreas Schweizer. (O. Klös)

Development of an Autonomous, Open-Source Observation Unit for Occultation and Variable Stars - Konrad Guhl, Herwig Diessner, Ansgar Schmidt (presented by Konrad Guhl)

Konrad introduced a project to develop an open-source platform that enables experienced amateur astronomers and professional researchers to participate in autonomous photometric monitoring of occultations and variable stars. It's a fully automated, optical observation unit that aims to create a cost-effective, flexible and scalable solution. He explained the first ideas for this project and invited a discussion on its aims and development.

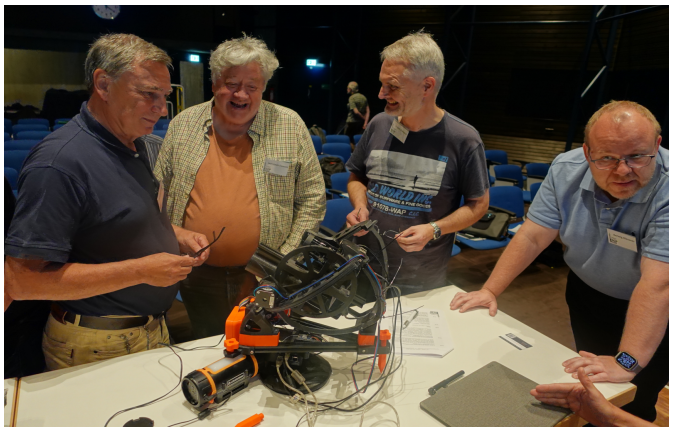

Figure 15. Konrad Guhl, Jean-Louis Dumont, Gregor Krannich and Herwig Diessner (from left to right) are excited about a 3D-printed remote station. (O. Klös)

ASE 14.10.2023 : Unfiltered annularity from the edge of path (presented by Jörg Schoppmeyer)

Jörg described how he observed the annular solar eclipse on 2023 October 14 from the northern edge of the annularity zone. He showed how he used an *unfiltered* high-quality refractor with a Herschel wedge and DSLR in video mode to record the maximum of the solar eclipse in white light in 4K resolution. Luca Quaglia and colleagues used his data to obtain a precise measurement of the solar diameter (see JOA 2024-02).

Figure 16. Jörg Schoppmeyer (right) during the Q&A after his presentation. Wolfgang Beisker (with microphone) leads the session. (O. Klös)

100 years of Sternwarte Stuttgart – 100 years of Occultation Astronomy (presented by Stefan Benz)

One of the oldest public observatories in southern Germany, Sternwarte Stuttgart on Uhlandshöhe hill above the city celebrated its 100th anniversary in 2022. Since its founding its volunteer members have hosted viewing sessions to promote astronomy to the general public. Stefan gave an overview of their scientific observing programmes, including lunar and solar eclipses, the transit of Venus, standard lunar and grazing occultations, asteroidal occultations and the Triton occultation.

Invitation to ESOP 44 (presented by Anna Marciniak)

Anna invited everyone to attend the next ESOP which will take place in Poznań, Poland from 22nd to 26th August, 2025. Poznań has good rail and airport links with major cities across Europe.

Closing of ESOP 43

Konrad Guhl and Andreas Eberle formally closed ESOP 43, thanking the local organising team for the smooth running of the conference, the very nice in-house catering during our sessions, and the contributions from all speakers and delegates. Andy reminded us of the timetable and meeting points for the upcoming social excursions on Monday and Tuesday.

The whole group then gathered together again and walked to Stuttgart city centre for an evening dinner at Carls Brauhaus. En route, Andreas pointed out a number of notable civic buildings and told us about their history.

Excursions

Monday 26th August 2024

Our morning pick-up point was near the Planetarium where we joined our coach for the drive to Schloss Solitude (Solitude Palace), sited in its own grounds on a hill overlooking a large swathe of countryside. It was built by Duke Carl Eugene for use as a summer residence and hunting retreat. After a look around the outside of the ornate buildings we continued our journey to Weil der Stadt to visit the birthplace house museum of Johannes Kepler.

We found the first display panels of the Johannes-Kepler-Planeten-weg but we didn't have time to walk to Neptune, 10.1 km away. Because of the size of our party, we were divided into two groups, one to visit the Kepler museum, the other to take a guided tour around this picturesque town, then vice versa. The museum is housed in a small half-timbered building where Kepler was born in 1571. Our guide took us through the property explaining the numerous displays which document the life of the famous astronomer-mathematician who lived through a time of religious conflict and the Reformation, astrology and astronomy, and played a major role in the scientific revolution. His contributions included his three laws of planetary motion and works on optics, and in his personal life he succeeded in defending his mother from accusations of witchcraft.

Figure 17. Kepler statue in the market place in Weil der Stadt (O. Klös)

Figure 18. The Stork Tower of Weil der Stadt. (A. Pratt)

Our walking tour guide led us through the streets of beautiful half-timbered houses, along a section of the city wall including the Stork Tower atop which is a distinctively large stork nest, and the Red Tower with grisly replicas of ancient instruments used for interrogations, torture and executions. Both groups then met up for an open-air buffet kindly arranged by our Stuttgart hosts.

Figure 19. Cordelia Eberle (left) and her team arranged a delicious open-air buffet. (O. Klös)

After lunch our coach took us to Kloster Hirsau, one of Germany's most famous 11th-century Benedictine Monasteries. Unfortunately, much of the St Peter and Paul monastery, its school and hunting lodge were reduced to rubble in the 1690s during the Nine Years War. Our guide walked us around the site and brought it back to life with her colourful descriptions of religious commitment in those times. The walls of the hunting lodge still stand, also the six-story Owl Tower with its friezes of people and animals. The Church of St. Aurelius was renovated in 1954.

We then drove to visit the ruins of Zavelstein castle, and after treating ourselves to ice creams, we explored the castle grounds. The central tower is well maintained and the climb up its central wooden staircase was rewarded with great views across the forested countryside. A leisurely walk took us to a restaurant for dinner.

Figure 20. Kloster Hirsau. (O. Klös)

Figure 21. The ruins of Zavelstein castle. (O. Klös)

Figure 22. Panoramic view of Zavelstein and the Black Forest from the tower of the castle (O. Klös)

That evening, en route back to Stuttgart, we visited the university's observatory which is a tower structure on its Pfaffenwald campus. Constructed in 1934 by Hermann Fellmeth (1888-1948), a board member of the Bosch company, it was his private observatory and after he passed away his family donated it to the university and it was renovated in the 1970s. He equipped it with a dual-mounted 300mm f/18 Cassegrain telescope and a 325mm f/10 Schupmann Medial telescope.

The latter is a special catadioptric designed in 1899 by Prof. Ludwig Schupmann (1851-1920) and manufactured by Merz in 1917, comprised of a biconvex objective, a field lens, a right-angled prism and a Mangin mirror. It is a fully achromatic telescope with minimal chromatic aberration and just a slight loss of 0.2 to 0.3 magnitudes. We were very pleased to be welcomed by Christian Wolter who gave us a detailed introduction to the largest working Schupmann Medial in Europe.

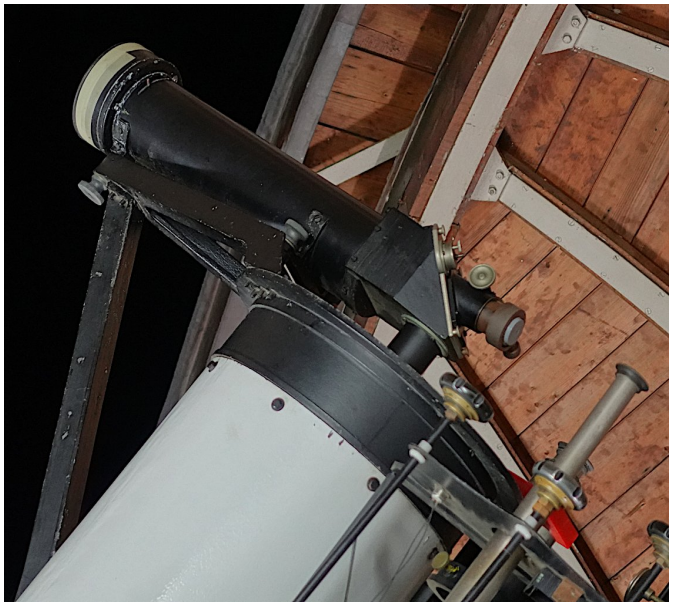

Figure 24 (top). The Schupmann Medial. (O. Klös)

Figure 23 (left). The observatory of Stuttgart university. (M. O'Connell)

Figure 25. Björn Kattentidt moves the telescope while Carsten Ziolek takes a picture of the Schupmann Medial. (O. Klös)

Tuesday 27th August 2024

We made our own way via S-Bahn (suburban railway) to the Mercedes-Benz Museum where our group entered this futuristic-looking building to spend a couple of hours learning about the engines invented by Carl Benz and Gottlieb Daimler, enabling the development of the first horseless carriages. The museum has numerous displays of these early exhibits, through to modern utility vehicles, trucks, sports cars and Formula One cars. Lunch was taken in the nearby VfB Stuttgart football club restaurant.

After lunch we took the S-Bahn to Esslingen for a guided walking tour around this picturesque town with its plentiful half-timbered houses. The highlight of our visit was to see the belltower and astronomical clock of the Altes Rathaus (Old Town Hall). Our guide told us about the complexities of the clock and its moving figures when they are in full action. After exploring more of its lovely, winding streets, sadly our trip had to come to an end. Small groups of us gradually said our goodbyes as we had to depart for our journeys home after a very enjoyable ESOP and we agreed to meet again next year in Poznań, Poland.

Figures 26, 27. Mercedes-Benz Museum in Stuttgart. (M. O'Connell)

Figure 28. Old Town Hall with astronomical clock in Esslingen. (M. O'Connell)

Further Reading

More about ESOP XLIII:
https://sternwarte.de/ESOP43

The astronomical clock of the Old Town Hall (in German):
https://de.wikipedia.org/wiki/Uhr_am_Alten_Rathaus_zu_Esslingen

Information about the Schupmann Medial telescope:

In German:
http://www.uni-stuttgart.de/sternwarte/
https://www.hochschulgruppe.uni-stuttgart.de/sternwarte/sternwarte/schuppmannsches-medial/
In English:
https://www.telescope-optics.net/schupmann_medial_telescope.htm
https://stellafane.org/history/modern/ludwig.html

Journal for Occultation Astronomy

IOTA's Mission

The International Occultation Timing Association, Inc was established to encourage and facilitate the observation of occultations and eclipses It provides predictions for grazing occultations of stars by the Moon and predictions for occultations of stars by asteroids and planets, information on observing equipment and techniques, and reports to the members of observations made.

The Journal for Occultation Astronomy (JOA) is published on behalf of IOTA, IOTA/ES and RASNZ and for the worldwide occultation astronomy community.

Worldwide Partners

Club Eclipse (France). . . . . www.astrosurf.com/club_eclipse
IOTA/EA (East Asia) . . . . . https://www.perc.it-chiba.ac.jp/iota-ea/wp/
IOTA-India . . . . . http://iota-india.in
IOTA/ME (Middle East) . . . . . www.iota-me.com
President: Atila Poro . . . . . iotamiddleeast@yahoo.com
LIADA (Latin America) . . . . . www.ocultacionesliada.wordpress.com
SOTAS (Stellar Occultation Timing Association Switzerland) . . . . . www.occultations.ch

Imprint

Publisher: International Occultation Timing Association/European Section e.V.
Am Brombeerhag 13, D-30459 Hannover, Germany
Responsible in Terms of the German Press Law (V.i.S.d.P.): Konrad Guhl
Editorial Board: Wolfgang Beisker, Oliver Klös, Alexander Pratt, Carles Schnabel, Christian Weber
Additional Reviewers: Dave Herald, Richard Miles, Roger Venable, Mike Kretlow Contact: joa@iota-es.de
Layout Artist: Oliver Klös Webmaster: Wolfgang Beisker
JOA Is Funded by Membership Fees (Year): IOTA: US$15.00 IOTA/ES: €20.00 RASNZ: NZ$35.00
Publication Dates: 4 times a year

Submission Deadline for JOA 2025-1: November 15

IOTA maintains the following web sites for your information and rapid notification of events:

www.occultations.org
www.iota-es.de
www.occultations.org.nz

These sites contain information about the organisation known as IOTA and provide information about joining.

The main page of occultations.org provides links to IOTA's major technical sites, as well as to the major IOTA sections, including those in Europe, East Asia, Middle East, Australia/New Zealand, and South America.

The technical sites hold definitions and information about all issues of occultation methods. It contains also results for all different phenomena. Occultations by the Moon, by planets, asteroids and TNOs are presented. Solar eclipses as a special kind of occultation can be found there as well results of other timely phenomena such as mutual events of satellites and lunar meteor impact flashes.

IOTA and IOTA/ES have an on-line archive of all issues of Occultation Newsletter, IOTA'S predecessor to JOA.

Journal for Occultation Astronomy
(ISSN 0737-6766) is published quarterly in the USA by the International Occultation Timing Association, Inc. (IOTA)
PO Box 20313, Fountain Hills, AZ 85269-0313
IOTA is a tax-exempt organization under sections 501(c)(3) and 509(a)(2) of the Internal Revenue Code USA, and is incorporated in the state of Texas. Copies are distributed electronically.